



# Rigid-flexible-thermal analysis of planar composite solar array with clearance joint considering torsional spring, latch mechanism and attitude controller

Yuanyuan Li · Cong Wang · Wenhui Huang

Received: 30 May 2018 / Accepted: 18 March 2019 / Published online: 13 April 2019  
© Springer Nature B.V. 2019

**Abstract** This paper establishes a thermal-structural coupling model of planar spacecraft system with large flexible composite solar array under nodal coordinate formulation and absolute nodal coordinate formulation framework. Perfect revolute joint is adopted as connection type to give the different influences from fixed constraint used in previous researches, and consequently, torsional spring, latch mechanism, and attitude controller are involved into the spacecraft system. Imperfect revolute joint is further introduced to investigate the coupling effects of thermal load, adjustment motion, and joint clearance on dynamics of the system, including spacecraft attitude, solar panel responses, and wear prediction. Results of six comparison models (with or without clearance joint, considering thermal environment, or adjustment motion, and considering both these two conditions) show that the coupling effect of thermal environment and overall motion brings dramatic and unmanageable shock to the system with clearance joint, that is no longer can be seen as a simple superposition of each single condition effect like the system with ideal joint, although the suspension damper property of clearance joint can weaken thermal-induced vibration

or motion induced vibration separately. For a period after attitude adjustment, wear depth of the system subjected to solar radiation is two orders of magnitude larger than that of the system without considering thermal environment. Joint clearance and thermal environment should be considered both; for on-orbit spacecraft system, the coupling effects of them are significant and non-ignorable for relevant mechanism design and performance analysis.

**Keywords** Rigid-flexible-thermal coupling · Solar array · Clearance joint · Wear prediction

## 1 Introduction

When a spacecraft is traveling in the orbit around the Earth, thermally induced vibrations may occur due to a sudden change of solar heat radiation [1]. The dramatic temperature changes on a surface of an appendage induce temperature gradients to generate thermal moment, that coupled with structural deformation and vibration of large flexible appendage may lead to unstable oscillation or thermal flutter of the on-orbit spacecraft [2,3]. The thermally induced responses of solar arrays result in attitude yaw of the whole spacecraft, a pointing jitter was also found when the Hubble Space Telescope was moving from shadow to sunlight [4]. Therefore, a complete dynamic analysis of thermal-structure-coupled solar array is one of the key problems

---

Y. Li (✉)  
Qian Xuesen Laboratory of Space Technology, China  
Academy of Space Technology, Beijing, People's Republic  
of China  
e-mail: liyy.hit@gmail.com

C. Wang · W. Huang  
School of Astronautics, Harbin Institute of Technology, Harbin,  
People's Republic of China

that need to be solved to guarantee the safety operation of spacecraft.

Recently, Li et al. [5] developed a thermal analysis model of composite solar array with complex structure to characterize the thermal response of the whole solar array system subjected to space heat flux. Different thermal environments, incident angles of solar radiation, and material properties of honeycomb panel are discussed to reveal the causes of thermally induced vibration [6]. Shen et al. [7] conducted a coupled thermal-structural analysis based on ANCF and examined thermally induced vibrations of a thin-walled tubular boom with a large rotation subjected to a sudden heating. Liu et al [8] proposed a rigid-flexible-thermal coupling model of an attitude maneuvering spacecraft. The thermal load includes not only the solar radiation flux, but also the earth-reflected heat radiation flux, earth-emitted heat radiation flux and the surface radiation. Liu et al [9] established rigid-flexible-thermal coupling dynamic model in terms of the Hamiltonian principle and non-constrained modes to study the interaction between the thermally induced vibration and attitude maneuver. Azadi et al [10] derived the governing equation of motion of an orbiting satellite with plate arrays and studied the effects of the heat radiation, radius of the orbit, piezoelectric voltages, and piezoelectric locations on the response of the system. Bai et al [11] investigated thermal behavior of a thin-walled deployable composite boom (DCB) in a space environment using ground thermal-vacuum test and FEA methods.

However, these thermal analysis studies simplified solar array system using fixed constraint to connect the spacecraft main body and solar panel. But the actual connection type of the system is hinge joint, and concomitantly some key mechanisms are must be involved, such as torsional spring, latch mechanism and attitude controller. Moreover, it has to be mentioned that joint clearance is inevitable and non-negligible existing in the hinged multi-body mechanism. In recent few decades, many researchers have paid attention to the effects of clearance on multi-body system using theoretical and experimental approaches in mechanical engineering [12–19].

Furthermore, clearance causes severe vibrations to affect attitude motion of spacecraft main body and deployment accuracy of flexible attachment [20]. The inner contact and impact force generated at clearance

joint may intensify wear performance to reduce system's reliability and stability, even lead to failure of the spacecraft missions. Li et al. [21] established the dynamics model of a space deployable mechanism with clearance using ADAMS to study the effects of clearance, damping, friction, gravity, and flexibility on the dynamic performance of a deployable mechanism in the deploying and locking processes. Li et al. [22] investigated the coupling effects of joint clearance and panel flexibility on the overall dynamic characteristics of a deployable solar array system. Li et al [23,24] established the dynamic equation of the solar array system by using single direction recursive construction method and the Jourdain's velocity variation principle to study the deployment and control of flexible solar array system considering joint friction. Furthermore, Li et al. [25] established the rigid-flexible coupling dynamics model of deployable solar array system with multiple clearance joints based on nodal coordinate formulation (NCF) and absolute nodal coordinate formulation (ANCF) to analyze and control satellite attitude under deployment disturbance, and presented significant guidance for the key parameters design of torsional spring, closed cable loops (CCL) configuration, and latch mechanism [26]. Obviously, these researches on the effect of clearance joint on the solar array system have not taken the thermal environment into account.

Therefore, this paper establishes a rigid-flexible-thermal coupling dynamic model of planar composite solar array with revolute joint and clearance revolute joint based on NCF-ANCF frame. To determine the model mechanism parameters and to reveal the connection effects of fixed constraint and revolute joint on on-orbit spacecraft subjected to solar radiation, three comparison models with different connection types and different torsional spring preloads are considered. More importantly, to analyze the coupling effects of joint clearance, thermal environment, and overall motion on the thermal-structural dynamics of the spacecraft with flexible solar panel system, six simulation models with different operation conditions are presented. This work considered completely these three of the main inducements of structure vibration, the thermal load of solar radiation, contact-impact force at clearance joint and adjustment motion of spacecraft attitude, which largely determine the dynamic performance of the whole system. Moreover, the effect of the existence of clearance joint on the thermal indeed

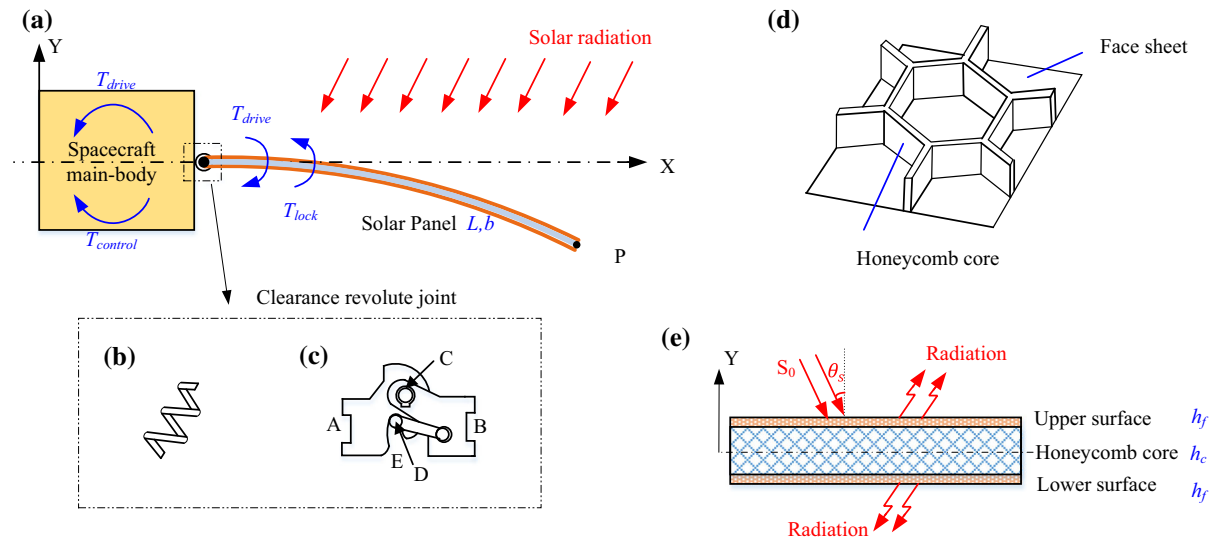


**Fig. 1** Model of solar array system used in this paper. **a** Deformation of solar array system under solar radiation; **b** torsional spring; **c** latch mechanism; **d** schematic of honeycomb core; **e** thermal analysis model of solar panel

vibration, and above all the effect of sunrise thermal load on wear prediction of solar array system with clearance joint will be also investigated in this paper.

The paper is organized as follows: Section 2 describes the spacecraft with solar arrays model subjected to thermal environment considering torsional springs, latch mechanism, attitude controller applied in this paper. Section 3 establishes rigid-flexible-thermal formulation consisting of the structure dynamics with thermal effect based on NCF-ANCF and thermal analysis based on FEM. Section 4 gives contact and friction models of planar revolute clearance joint under NCF-ANCF framework, and uses Archard’s wear model to describe wear calculation. Section 5 gives computational solutions to solve equations of motion of planar rigid-flexible multi-body system with clearance joints by using Generalized- $\alpha$  method. Section 6 gives calculation parameters of the solar array model considering thermal environment. In Sect. 7, simulation model parameters are determined and different connection types’ effect are discussed. Numerical results are presented to discuss the coupling effects of joint clearance, thermal load and adjustment motion on satellite attitude, solar panel and wear prediction. Finally, the main conclusions are drawn in Sect. 8.

## 2 Description of a solar array model considering thermal environment

Figure 1 shows a typical spacecraft model with deployed solar array under solar radiation. Moreover, the solar array also emits heat radiation to deep space. The spacecraft model adopted in this paper (Fig. 1a) consists of one rigid main body and one flexible composite panel connected by a clearance revolute joint. When the spacecraft is launched into the orbit, preloaded torsional spring mechanism (see Fig. 1b) provides driving force to deploy folded panels and latch mechanism (see Fig. 1c) latches the solar panel at expected plane position. These latch mechanism and torsional spring mechanism are located at revolute joint. The cell of honeycomb core is given in Fig. 1d.

### 2.1 Torsional spring mechanism

The driving torque generated from torsional spring mechanism can be expressed as [4–7]

$$T_{drive} = K_s(\theta_{pre} - \theta) \tag{1}$$

where  $K_s$  is the torsion stiffness of torsion spring;  $\theta_{pre}$  and  $\theta$  are the preload angle of torsion spring, respectively. Here,  $\theta = 0.5\pi$ , at the deployment position.

### 2.2 Latch mechanism

As shown in Fig. 1c, the revolute joint C connects spacecraft main body A and solar panel B separately; when the pin D slides into the groove E, the latch mechanism is activated to lock the two bodies.

A BISTOP function is introduced to present the equivalent moment  $T_{lock}$  in the latch mechanism [23–26]. BISTOP function allows free motion between  $x_1$  and  $x_2$  at which point the contact function begins to push the joint back toward the expect center angle. The latch torque can be expressed as

$$T_{lock} = \text{BISTOP}(\theta, \dot{\theta}, 89.5^\circ, 90.5^\circ, 1 \times 10^5, 1 \times 10^3, 1.5, 0.1^\circ) \tag{2}$$

where  $\theta$  is the deployment angle at joint,  $\dot{\theta}$  is the rotation velocity.

Here

$$\text{BISTOP}(\theta, \dot{\theta}, x_1, x_2, K_{bs}, e, C_{max}, d) = \begin{cases} \text{if } \theta_i < x_1 : \\ \text{Max}(K_{bs}(x_1 - \theta)^e - \dot{\theta} \text{step}(\theta, x_1 - d, C_{max}, x_1, 0), 0) \\ \text{if } \theta_i > x_2 : \\ \text{Min}(-K_{bs}(\theta - x_2)^e - \dot{\theta} \text{step}(\theta, x_2, 0, x_2 - d, C_{max}), 0) \end{cases} \tag{3}$$

$$\text{step}(\theta, x_3, h_1, x_4, h_2) = \begin{cases} \text{if } \theta < x_3 : 0 \\ \text{if } x_3 \leq \theta \leq x_4 : \\ h_1 + (h_2 - h_1) \left( \frac{\theta - x_3}{x_4 - x_3} \right)^2 \left( 3 - 2 \times \frac{\theta - x_3}{x_4 - x_3} \right) \\ \text{if } \theta_i > x_4 : 1 \end{cases} \tag{4}$$

where  $K_{bs}$  and  $C_{max}$  are the stiffness and damping coefficients of the corresponding latch mechanism, respectively;  $e$  is an exponent;  $d$  is the distance depth. The step function approximates the Heaviside step function with a cubic polynomial increases from  $h_1$  to  $h_2$ .

### 2.3 Controller design

Controller should be designed to adjust the attitude change of the spacecraft due to the disturbance or motion during the mission. In this paper, classical proportional–differential (PD) control method is selected to design the controller of attitude adjusting. The PD control can be expressed as

$$\mathbf{F}(t) = \mathbf{K}_p \cdot (\mathbf{e}_{ref} - \mathbf{e}) + \mathbf{K}_d \cdot (\dot{\mathbf{e}}_{ref} - \dot{\mathbf{e}}) \tag{5}$$

where the PD tuner proportional and differential gains  $\mathbf{K}_p$  and  $\mathbf{K}_d$  are chosen as  $K_p = 1000$  and  $K_d = 200$ .

$\mathbf{e}_{ref}$  and  $\mathbf{e}$  are desired attitude and real attitude of the spacecraft main body.  $\dot{\mathbf{e}}_{ref}$  and  $\dot{\mathbf{e}}$  are time differential of  $\mathbf{e}_{ref}$  and  $\mathbf{e}$ .

### 2.4 Thermal environment

The analysis considers the case of 600-km circular orbit whose orbital plane lies in the ecliptic, which is a typical low Earth orbital satellite altitude. The incident solar heat flux history is given as: at  $t = 0$  s, the solar panel is in total shadow ( $S_0 = 0 \text{ W/m}^2$ ), and at  $t = 10$  s, it enters the penumbra and begins the transition to full sunlight ( $S_0 = 1350 \text{ W/m}^2$ ). The transition time between total shadow and full sunlight is approximately 8.5 s [27].

As illustrated in Fig. 1e, the heat flux absorbed by the upper surface conducts along the panel thickness. Meanwhile, the heat flow radiation is emitted to space on the upper and lower surfaces. There is no heat conduction between the main body and panel. The heat convection is also neglected because of high-vacuum and low-pressure space environment. The black-body radiating temperature of the space environment is considered as 0 K in the thermal analysis, and the initial temperature  $T_0$  is set to be 290 K for the solar panel.

## 3 Coupled rigid-flexible-thermal formulation based on NCF-ANCF

### 3.1 Structure dynamics with thermal effect

In this work, the spacecraft main body is described as rigid part by using nodal coordinate formulation (NCF) and the composited solar panel is described as flexible part by using the absolute nodal coordinate formulation (ANCF). ANCF proposed by Shabana [28] can accurately model a deformable body with large deformation and motion, and there are some successful applications to characterize the large flexible attachment of spacecraft [7, 25, 29, 30]. However, to ensure simulation accuracy and computation efficiency, it is necessary to deduce generalized elastic force matrix of the system considering thermal effect with reasonable simplification based on ANCF as shown in the following section.

For a planar ANCF-based deformable beam element as shown in Fig. 2, a global position vector  $\mathbf{r}$  of an arbi-

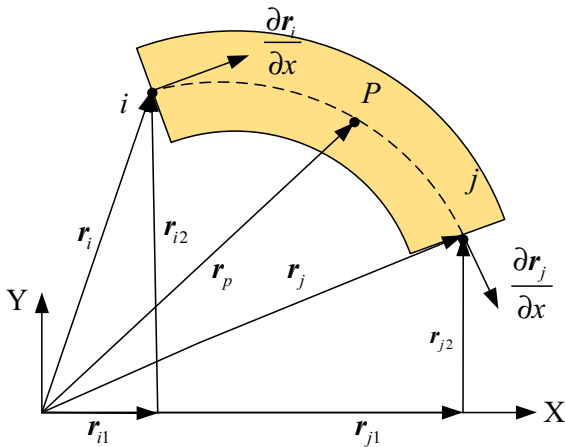


Fig. 2 Planar ANCF element

bitrary point P on the neutral axis of a two-dimensional beam element in ANCF is given by

$$\mathbf{r} = \begin{bmatrix} r_1 \\ r_2 \end{bmatrix} = \mathbf{S}\mathbf{e} \tag{6}$$

where  $\mathbf{S}$  is the global shape function and  $\mathbf{e}$  is the vector of element nodal coordinates.

$$\mathbf{S} = \begin{bmatrix} s_1, 0, s_2l, 0, s_3, 0, s_4l, 0 \\ 0, s_1, 0, s_2l, 0, s_3, 0, s_4l \end{bmatrix} \tag{7}$$

where the functions  $s_i = s_i(\xi)$  are defined as

$$\begin{aligned} s_1 &= 1 - 3\xi^2 + 2\xi^3, & s_2 &= \xi - 2\xi^2 + \xi^3, \\ s_3 &= 3\xi^2 - 2\xi^3, & s_4 &= \xi^3 - \xi^2. \end{aligned} \tag{8}$$

and  $\xi = x/l$ .  $l$  the original length of the beam element, and  $x$  is the coordinate of an arbitrary point on the element in the undeformed configuration.

The vector of beam element nodal coordinates  $\mathbf{e}$  is defined as

$$\mathbf{e} = [e_1, e_2, e_3, e_4, e_5, e_6, e_7, e_8] \tag{9}$$

This vector of absolute nodal coordinates includes the global displacements

$$\begin{aligned} e_1 &= r_1|_{x=0}, & e_2 &= r_2|_{x=0}, \\ e_5 &= r_1|_{x=l}, & e_6 &= r_2|_{x=l}. \end{aligned} \tag{10}$$

and the global slopes of the element nodes, that are defined as

$$\begin{aligned} e_3 &= \frac{\partial r_1}{\partial x}|_{x=0}, & e_4 &= \frac{\partial r_2}{\partial x}|_{x=0}, \\ e_7 &= \frac{\partial r_1}{\partial x}|_{x=l}, & e_8 &= \frac{\partial r_2}{\partial x}|_{x=l}. \end{aligned} \tag{11}$$

The kinetic energy of the beam element is defined as follows:

$$\begin{aligned} T &= \frac{1}{2} \int_V \rho \dot{\mathbf{r}}^T \dot{\mathbf{r}} dV \\ &= \frac{1}{2} \dot{\mathbf{e}}^T \left( \int_V \rho \mathbf{S}^T \mathbf{S} dV \right) \dot{\mathbf{e}} = \frac{1}{2} \dot{\mathbf{e}}^T \mathbf{M} \dot{\mathbf{e}} \end{aligned} \tag{12}$$

where  $\mathbf{M} = \int_V \rho \mathbf{S}^T \mathbf{S} dV$  is a constant mass matrix,  $V$  is the element volume,  $\rho$  is the mass density.

For the Euler–Bernoulli beam, the beam element cross sections are assumed to remain plane and perpendicular to the beam centerline. The longitudinal strain energy of the element including thermal effect can be expressed as

$$U_l = \frac{1}{2} \int_0^l EA(\varepsilon_l - \varepsilon_{Tl})^2 dx \tag{13}$$

where  $E$  is the Young modulus,  $A$  is the cross-sectional area of the beam,  $\varepsilon_l$  is the longitudinal strain, and  $\varepsilon_{Tl}$  is the longitudinal thermal strain.

Here, the longitudinal strain  $\varepsilon_l$  is defined by

$$\varepsilon_l = \frac{1}{2}(f^2 - 1) = \frac{1}{2}(\mathbf{r}^T \mathbf{r}' - 1) \tag{14}$$

The quantity  $\sqrt{\mathbf{r}^T \mathbf{r}'}$  represents the deformation gradient  $f$  for longitudinal deformations.

And the thermal-induced longitudinal strain  $\varepsilon_{Tl}$  is expressed as

$$\varepsilon_{Tl} = \alpha_T(\bar{T} - T_0) \tag{15}$$

where  $\alpha_T$  is the coefficient of thermal expansion,  $\bar{T}$  is the average temperature over the cross section, and  $T_0$  is a reference temperature.

For convenience, the following matrices are defined:

$$\mathbf{S}_l = \mathbf{S}'^T \mathbf{S}' = \frac{1}{l^2} \mathbf{S}_{,\xi}^T \mathbf{S}_{,\xi} \tag{16}$$

$$\bar{\mathbf{S}}_l = \int_0^1 \mathbf{S}_l d\xi \tag{17}$$

where  $\mathbf{S}_{,\xi}$  is the derivative of the shape function  $\mathbf{S}$  with respect to the dimensionless parameter  $\xi$ . using the definition of  $\mathbf{S}_l$ , the longitudinal strain can be written as

$$\varepsilon_l = \frac{1}{2}(\mathbf{e}^T \mathbf{S}_l \mathbf{e} - 1) \tag{18}$$

From this equation, it is clear that

$$\left(\frac{\partial \varepsilon_l}{\partial \mathbf{e}}\right)^T = \mathbf{S}_l \mathbf{e} \tag{19}$$

The longitudinal elastic force  $\mathbf{Q}_l$  is defined as

$$\mathbf{Q}_l = \left(\frac{\partial U_l}{\partial \mathbf{e}}\right)^T = \int_0^l EA\varepsilon_l \mathbf{S}_l \mathbf{e} dx - \int_0^l EA\varepsilon_{Tl} \mathbf{S}_l \mathbf{e} dx. \tag{20}$$

Then the longitudinal elastic force can be expressed as

$$\mathbf{Q}_l = \mathbf{K}_l \mathbf{e} + \mathbf{K}_{Tl} \mathbf{e}. \tag{21}$$

Assuming  $E$  and  $A$  as constants, the stiffness matrix  $K_l$  can be written as

$$K_l = \frac{1}{2}EA \left[ \int_0^l (\mathbf{S}_l \mathbf{e} \mathbf{e}^T \mathbf{S}_l) d\xi - \int_0^l \mathbf{S}_l d\xi \right], \tag{22}$$

And the stiffness matrix related to thermal  $K_{Tl}$  can be written as

$$K_{Tl} = - \int_0^l EA \varepsilon_{Tl} \mathbf{S}_l d\xi. \tag{23}$$

The transverse strain energy of the beam element with thermal effect is given by

$$U_t = \frac{1}{2} \int_V E (\varepsilon_t - \varepsilon_{Tt})^2 dx \approx \frac{1}{2} \int_V E \varepsilon_t^2 dv - \int_V E \varepsilon_t \varepsilon_{Tt} dv = \frac{1}{2} \int_0^l M \kappa dx - \int_0^l M_T \kappa dx \tag{24}$$

The effect of bending can be introduced using the equation

$$M = EI \kappa \tag{25}$$

where  $I$  is the second moment of area. The curvature  $\kappa$  of a curve described in the parametric form of equation

$$\kappa = \left| \frac{d^2 \mathbf{r}}{ds^2} \right| \tag{26}$$

The curvature of equation can also be written as

$$\kappa = \frac{|\mathbf{r}' \times \mathbf{r}''|}{|\mathbf{r}'|^3} \tag{27}$$

For two-dimensional problems, the equation can be written as

$$\kappa = \frac{\mathbf{r}'^T \tilde{\mathbf{I}} \mathbf{r}''}{|\mathbf{r}'^T \tilde{\mathbf{I}} \mathbf{r}'|^{3/2}} = \frac{\mathbf{r}''^T \tilde{\mathbf{I}} \mathbf{r}'}{f^3} \tag{28}$$

where  $\tilde{\mathbf{I}} = \begin{bmatrix} 0, & -1 \\ 1, & 0 \end{bmatrix}$ .

Then the curvature can be written as

$$\kappa = \frac{\mathbf{e}^T \mathbf{S}_t \mathbf{e}}{f^3}. \tag{29}$$

where the symmetric matrix  $\mathbf{S}_t$  is a sparse matrix with a very simple structure.

$$\mathbf{S}_t = \frac{1}{2} (\hat{\mathbf{S}}_t + \hat{\mathbf{S}}_t^T). \tag{30}$$

where the matrix  $\hat{\mathbf{S}}_t$  is defined as

$$\hat{\mathbf{S}}_t = \mathbf{S}^T \tilde{\mathbf{I}} \mathbf{S}'' = \frac{1}{l^3} S_{,\xi}^T \tilde{I} S_{,\xi\xi}. \tag{31}$$

And the thermal moment  $M_T$  is defined as

$$M_T = \int_A E \alpha_T (\bar{T} - T) y dA \tag{32}$$

The equation of  $\kappa$ , however, will lead to a complex expression for the elastic forces. This expression can be significantly simplified if the longitudinal deformation within the element is assumed constant in developing the transverse elastic forces. In this case, the deformation gradient  $f$  is assumed equal to a constant value  $\bar{f}$ :

$$\frac{ds}{dx} = \bar{f} = \text{const} \tag{33}$$

$$\bar{f} = \sqrt{\int_0^1 f^2 d\xi} = \sqrt{\int_0^1 \mathbf{r}'^T \mathbf{r}' d\xi} = \sqrt{\mathbf{e}^T \tilde{\mathbf{S}}_l \mathbf{e}}. \tag{34}$$

and consequently

$$\kappa^2 = \frac{1}{\bar{f}^4} \mathbf{e}^T \mathbf{S}''^T \mathbf{S}'' \mathbf{e} \tag{35}$$

The vector of the elastic forces due to the transverse deformation is given by

$$\mathbf{Q}_t = \left(\frac{\partial U_t}{\partial \mathbf{e}}\right)^T = \mathbf{K}_t \mathbf{e} + \mathbf{K}_{Tt} \mathbf{e} \tag{36}$$

$$\mathbf{K}_t = EI \left[ \frac{1}{\bar{f}^4} \int_0^1 \mathbf{S}''^T \mathbf{S}'' d\xi - \frac{2}{\bar{f}^6} \int_0^1 \mathbf{e}^T \mathbf{S}''^T \mathbf{S}'' \mathbf{e} d\xi \tilde{\mathbf{S}}_l \right] \tag{37}$$

$$\mathbf{K}_{Tt} = -M_T l \left[ \frac{2}{\bar{f}^3} \int_0^1 \mathbf{S}_t d\xi - \frac{3}{\bar{f}^5} \int_0^1 \mathbf{e}^T \mathbf{S}_t \mathbf{e} d\xi \tilde{\mathbf{S}}_l \right] \tag{38}$$



### 3.2 Thermal analysis

In the coupled thermal-structural analysis, the heat flux  $q_s$  is related to the structural deformation by

$$q_s = \alpha_s \cdot S = \alpha_s \cdot S_0 \cdot \cos\theta_s \tag{39}$$

where  $\alpha_s$  is the surface absorptivity of the upper surface,  $S_0$  is the value of the solar radiation, and  $\theta_s$  is the intersection angle between the solar radiation heat flux  $S_0$  and the absorbed heat flux  $S$  (see Fig. 1e).

The heat flux absorbed by the upper surface is assumed to only conduct through the panel thickness [7,9,31]. The transient one-dimensional heat conduction equation for the face sheet or honeycomb core of solar panel is written as

$$\rho_{f(c)}c_{f(c)} \frac{\partial T(x, y, t)}{\partial t} = \kappa_{f(c)} \frac{\partial^2 T(x, y, t)}{\partial^2 y} \tag{40}$$

where  $\rho_{f(c)}$ ,  $c_{f(c)}$  and  $\kappa_{f(c)}$  are the density, the specific heat and the thermal conductivity of the face sheet or honeycomb core, respectively.

The initial condition for this thermal model is

$$T(x, y, t)|_{t=0} = T_0, \quad 0 \leq x \leq L, \quad -\frac{h}{2} \leq y \leq \frac{h}{2} \tag{41}$$

Two boundary conditions must be provided for the upper surface ( $y = \frac{h}{2}$ ) and the lower surface ( $y = -\frac{h}{2}$ ) to solve the partial differential heat equation, as given by

$$-k_f \frac{\partial T(x, y, t)}{\partial y} \Big|_{y=\frac{h}{2}} = \alpha_s S - \xi_{up}\sigma_T T^4(x, y, t) \tag{42}$$

$$-k_f \frac{\partial T(x, y, t)}{\partial y} \Big|_{y=-\frac{h}{2}} = -\xi_{low}\sigma_T T^4(x, y, t). \tag{43}$$

where  $\xi_{up}$  and  $\xi_{low}$  are emissivity of the upper and lower surfaces.  $\sigma_T = 5.67 \times 10^{-8} \text{W m}^{-2} \text{K}^{-4}$  is the Stefan-Boltzmann constant.

Finite element analysis was used to predict the thermal response of a solar panel subject to orbital eclipse transition heating [7,9]. The heat conduction equation of one finite element with boundary conditions is deduced by

$$\mathbf{C}\dot{\mathbf{T}} + \mathbf{K}_c\mathbf{T} = \mathbf{R}_r(\mathbf{e}) + \mathbf{R}_T(\mathbf{T}) \tag{44}$$

where  $\mathbf{C}$  is the element capacitance matrix and the coefficients  $\mathbf{K}_c$  is element conduction matrix. The vector  $\mathbf{R}_r$  is the heat loading vector related to the structural deformation and  $\mathbf{R}_T$  is the heat loading vector due to surface

radiant heating. Here  $\dot{\mathbf{T}} = \frac{\partial \mathbf{T}}{\partial t}$  and  $\mathbf{T}$  is the unknown nodal temperature.

These coefficients in Eq. (44) for a two-node element are expressed by

$$\begin{aligned} \mathbf{C} &= \frac{\rho_{f(c)}c_{f(c)}h_e}{2} \begin{bmatrix} 1 & 0 \\ 0 & 1 \end{bmatrix}, & \mathbf{K}_c &= \frac{\kappa}{h_e} \begin{bmatrix} 1 & -1 \\ -1 & 1 \end{bmatrix}, \\ \mathbf{R}_r^{\text{up}} &= \alpha_s S(e) \begin{bmatrix} 1 \\ 0 \end{bmatrix}, & \mathbf{R}_T^{\text{up}} &= -\xi_{up}\sigma_T \begin{bmatrix} T_{\text{up}}(t)^4 \\ 0 \end{bmatrix}, \\ \mathbf{R}_T^{\text{low}} &= -\xi_{low}\sigma_T \begin{bmatrix} 0 \\ T_{\text{low}}(t)^4 \end{bmatrix}. \end{aligned} \tag{45}$$

where  $h_e$  is the thickness of the element is thermal analysis.  $T_{\text{up}}(t)$  and  $T_{\text{low}}(t)$  are temperature of upper surface and lower surface of solar panel at time  $t$ , respectively.

The stability criteria of heat conduction equation is given by

$$\frac{k_{f(c)}}{\rho_{f(c)}c_{f(c)}} \frac{\Delta t}{(h_e)^2} \leq \frac{1}{2}. \tag{46}$$

where  $\Delta t$  is time increment for iterative computation.

### 4 Clearance joint model

This subsection establishes a mathematical model of revolute clearance joint to represent the normal contact force and tangential friction force in the equations of motion of rigid-flexible multi-body system. Figure 3 gives the sleeve and hinge pin of a revolute clearance joint in the NCF-ANCF framework.

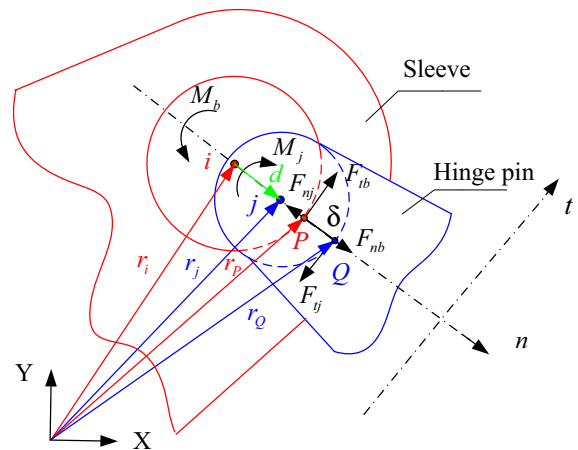


Fig. 3 A revolute clearance joint in the NCF-ANCF framework

#### 4.1 Clearance joint model in the NCF-ANCF framework.

Based on the NCF and ANCF, nodes  $i$  and  $j$ , respectively, indicate the center of the sleeve and the center of the hinge pin. The eccentricity vector  $\mathbf{d}$  represent the difference between the node  $i$  and  $j$ , and it can be expressed as

$$\mathbf{d} = \mathbf{r}_j - \mathbf{r}_i \tag{47}$$

The vector  $\mathbf{n}$  represents the normal direction of the collision surfaces between the sleeve and the hinge pin; accordingly, the vector  $\mathbf{t}$  represents the tangential direction. Obviously, the vector  $\mathbf{n}$  is the unit eccentricity vector. It can be expressed by

$$\mathbf{n} = \frac{\mathbf{d}}{\|\mathbf{d}\|} \tag{48}$$

Then the penetration depth due to local deformation is evaluated as

$$\delta = \|\mathbf{d}\| - c \tag{49}$$

where  $\delta$  is represented by the distance between  $P$  and  $Q$  in Fig. 5.  $c$  denotes radial clearance value, which is equal to  $R_s - R_p$ . Here  $R_s$  and  $R_p$ , respectively, denote the radius of the sleeve and the radius of the hinge pin.

Point  $P$  is the contact point on sleeve body and point  $Q$  is the contact point on hinge pin body. Here are the position expressions of point  $P$  and  $Q$ , respectively, as

$$\begin{aligned} \mathbf{r}_P &= \mathbf{r}_i + \mathbf{n}R_s, \\ \mathbf{r}_Q &= \mathbf{r}_j + \mathbf{n}R_p. \end{aligned} \tag{50}$$

The velocity of these two contact points  $P$  and  $Q$  under the global coordinate system can be obtained by taking derivative of Eq. (58) as

$$\begin{aligned} \dot{\mathbf{r}}_P &= \dot{\mathbf{r}}_i + \dot{\mathbf{n}}R_s, \\ \dot{\mathbf{r}}_Q &= \dot{\mathbf{r}}_j + \dot{\mathbf{n}}R_p. \end{aligned} \tag{51}$$

The normal velocity and tangential velocity need to be deduced to calculate the normal contact force and tangential friction force. Thus, the relative normal velocity can be expressed as

$$\mathbf{v}_n = [(\mathbf{r}_P - \mathbf{r}_Q)^T \mathbf{n}] \tag{52}$$

and the corresponding tangent velocity can be obtained by

$$\mathbf{v}_t = (\dot{\mathbf{r}}_P - \dot{\mathbf{r}}_Q) - \mathbf{v}_n \tag{53}$$

In order to indicate the contact, impact and friction forces under the NCF and ANCF framework, the forces

that acted on the contact points  $P$  and  $Q$  should be transformed into the forces that acted at the nodes  $i$  and  $j$ . In addition, the torques that applied on the sleeve center node  $i$  and hinge pin center node  $j$  can be obtained respectively by

$$\begin{aligned} \mathbf{M}_i &= \mathbf{F}_{ti} \times \mathbf{R}_i, \\ \mathbf{M}_j &= \mathbf{F}_{tj} \times \mathbf{R}_j. \end{aligned} \tag{54}$$

Accordingly, normal contact force and tangential friction force can be obtained based on some appropriate contact and friction laws as generalized forces in the equations of motion of the solar array system.

#### 4.2 Contact forces in revolute clearance joint

This paper selects Lankarani and Nikravesh model [32] to evaluate the normal contact forces, since it also considers energy dissipation in the contact-impact process. Besides, compared to other estimated contact force models, this model shows better ability to obtain accurate results [12]. It has been used for numerous studies [13–15] and has been validated by experimental studies [16]. The model is given as

$$\mathbf{F}_N = \left( K \delta^n \left[ 1 + \frac{3(1 - C_e^2) \dot{\delta}}{4\dot{\delta}^{(-)}} \right] \right) \mathbf{n} \tag{55}$$

where  $F_N$  is the normal contact force,  $K$  is the equivalent stiffness;  $\delta$  is the penetration depth of the contacting bodies; the exponent  $n$  selects 1.5 for metallic surfaces;  $\dot{\delta}$  and  $\dot{\delta}^{(-)}$  are the relative impact velocity and the initial impact velocity, respectively.  $C_e$  is the restitution coefficient; here  $K$  depends on the material properties and the shape of the contacting surfaces, which is expressed as:

$$\begin{aligned} K &= \frac{4}{3\pi(\sigma_s + \sigma_p)} \left[ \frac{R_s R_p}{R_s - R_p} \right]^{\frac{1}{2}} \\ \sigma_k &= \frac{1 - \nu_k^2}{\pi E_k} \quad (k = s, p) \end{aligned} \tag{56}$$

where  $R_s$  and  $R_p$  are the radii of the sleeve and pin, respectively.  $E_k$  and  $\nu_k$  are the Young's modulus and Poisson's ratio associated with each component.

#### 4.3 Friction force in revolute clearance joint

In general, Coulomb friction model is widely selected to calculate the friction force in contact-impact process. However, to prevent the numerical difficulties happen



near the tangential velocity equal to zero, a modified Coulomb’s friction law is selected to represent the friction response in this work, which has been used for numerous studies [15, 17, 18]. Besides, the comparative investigation of effects of the Lund–Grenoble model and the modified Coulomb model on the system dynamics shows that the moments obtained via these two friction models are very close [19]. Thus, the friction model selected here is denoted as,

$$F_T = -c_f c_d F_N \frac{v_t}{\|v_t\|} \tag{57}$$

where  $c_f$  is the friction coefficient,  $v_t$  is the relative tangential velocity. And dynamic correction coefficient  $c_d$  is given by

$$c_d = \begin{cases} 0 & \text{if } \|v_t\| \leq v_0 \\ \frac{\|v_t\| - v_0}{v_1 - v_0} & \text{if } v_0 \leq \|v_t\| \leq v_1 \\ 1 & \text{if } \|v_t\| \geq v_1 \end{cases} \tag{58}$$

where  $v_0$  and  $v_1$  are given tolerances for the tangential velocity. The parameters are adopted according to literature [19]. The dynamic correction factor  $c_d$  can prevent friction force from direction changes at almost null values of the tangential velocity.

#### 4.4 Wear depth

In the case of the revolute clearance joint components, the wear would occur when sleeve and pin are in contact and make relative motion. The most frequently used model is the Archard’s wear model [33], which is widely used by a great deal of works to predict wear pattern occurring in the clearance joint [34, 35]. Thus, this paper selects the Archard’s wear model to calculate the wear of revolute clearance joint in solar array systems. The Archard’s wear calculation formula is described as,

$$V = K_W \frac{F_N S}{H} \tag{59}$$

where  $V$  is wear volume;  $K_W$  is dimensionless wear coefficient;  $F_N$  is external load;  $H$  hardness of materials; and  $S$  is relative slippage distance of contact surface.

When the wear depth deserves more interest than the wear volume, Eq. (59) can be denoted as,

$$h = \frac{K_W}{H} p S \tag{60}$$

where  $h$  represents the wear depth and  $p$  indicates the normal contact pressure. The wear coefficient is adopted according to literature [35].

### 5 Computational solutions for dynamical equation

Under the NCF-ANCF framework, the assembly of these planar rigid and flexible elements can be operated in accord with the traditional finite element method. Thus, the nodal coordinates of each element  $q_e$  can be transformed into the generalized coordinates of the whole rigid-flexible coupling multi-body system  $q$ . The dynamics equation of multi-body system is calculated using the Lagrange multiplier method. The equations of motion for a rigid-flexible coupling solar array system can be obtained in a compact form as

$$\begin{pmatrix} M & \Phi_q^T \\ \Phi_q^T & 0 \end{pmatrix} \begin{pmatrix} \ddot{q} \\ \lambda \end{pmatrix} = \begin{pmatrix} Q_{ex} + Q_e \\ -(\Phi_q \dot{q})_q \dot{q} - 2\Phi_{qt} - \Phi_{tt} \end{pmatrix} \tag{61}$$

where  $M$  is the generalized mass matrix of the multi-body system, respectively.  $\ddot{q}$  is the generalized acceleration vectors matrix.  $\Phi_q$  is the Jacobi matrix of constraint equation.  $\lambda$  is the Lagrange multiplier column matrix,  $Q_{ex}$  is the generalized external force matrix composed of driving force, torsional spring torque, lock torque, controlling torque, contact force and friction force. When the contact is accurately detected, the contact-impact force is introduced.  $Q_e$  is the elastic force matrix given by  $Q_l$  and  $Q_f$ .

The coupled thermal-structural analysis composed of the nonlinear equations (61) and (44) in each time step is solved by the generalized- $\alpha$  method [7, 30] inter-actively.

### 6 Numerical model and parameters

A typical deployable solar array system composed of a rigid main body, and one composited flexible panel is modeled based on the NCF-ANCF formulation considering thermal environment. In the simulation example, the satellite is a rectangular rigid body with mass  $m_b = 2000$  kg. The length, width, and the height of the satellite are all equal to 1 m. The flexible solar array is a composited plate. The geometric and material properties are given in the Table 1 [23]. The flexible panel is divided into 8 elements, so the whole multi-body system has 40 degrees of freedom based on NCF-ANCF in this paper. Besides, the materials of hinge pin and sleeve are steel and brass, respectively. The radius of hinge pin is set as  $r_p = 0.01$  m, and the radius of sleeve is set as  $r_s = 0.0102$  m. for the torsional spring mechanism, the torsional stiffness of spring  $K_s$  is 0.075

**Table 1** Geometric and material parameters of the flexible plate

|  | Face sheet            | Honeycomb core        |
|--|-----------------------|-----------------------|
| Length of the plate $L$ (m)  | 8.0                   |                       |
| Width of the plate $b$ (m)   | 2.0                   |                       |
| Thickness $h_f, h_c$ (m)   | $2.54 \times 10^{-4}$ | 0.0254                |
| Mass density $\rho_f, \rho_c$ ( $\text{kg} \times \text{m}^{-3}$ )                     | 2800                  | 30                    |
| Elastic modulus of aluminum $E$ (Pa)   | $6.89 \times 10^{10}$ | $4.23 \times 10^5$    |
| Thermal expansion coefficient $\alpha_T$ ( $\text{K}^{-1}$ )                           | $2.32 \times 10^{-5}$ | $2.38 \times 10^{-5}$ |
| Specific heat $c$ ( $\text{J} \times \text{kg}^{-1} \times \text{K}^{-1}$ )            | 960                   | 920                   |
| Thermal conductivity $\kappa$ ( $\text{W} \times \text{m}^{-1} \times \text{K}^{-1}$ ) | 168                   | 1.2                   |
| Absorptivity of upper face sheet $\alpha_s$  | 0.79                  | –                     |
| Emissivity $\xi_{\text{up}}, \xi_{\text{low}}$   | 0.81, 0.86            | –                     |

N m/rad in Eq. (1). For the clearance joint, the coefficients of restitution  $C_e$  is 0.9 and contact stiffness  $K$  is  $7.39 \times 10^{10} \text{N/m}^{3/2}$  in Eq. (55). The friction coefficient  $c_f$  is 0.15 in Eq. (57).

To study the effect of connection type between spacecraft main body and panel on attitude yaw and dynamic response of solar array, and to determine the mechanism parameters of the whole system, three comparison models subjected to solar radiation with attitude controller are established in Sect. 7.1. Model I is connected by fixed constraint, and Model II is connected by revolute joint and the preload angle of torsional spring is set as  $0.5\pi$ . To make sure the solar panel can be derived to reach the designated position, there are usually a certain amount of the preload margin. So, the preload angle of torsional spring of Model III is set as  $0.75\pi$ .

To study the effects of thermal environment, attitude adjustment and joint clearance on the dynamic response of the whole system, six comparison models are established in this paper. Model IJ-T: system with ideal joint under thermal load; Model IJ-M: system with ideal joint considering motion; Model IJ-T-M: system with ideal joint considering motion under thermal load; Model CJ-T: system with clearance joint under thermal load; Model CJ-M: system with clearance joint considering motion; Model CJ-T-M: system with clearance joint considering motion under thermal load.

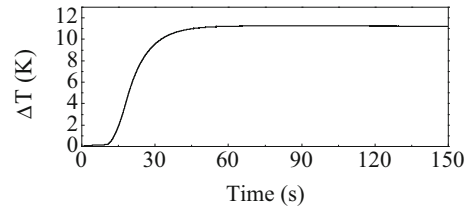


**Fig. 4** Temperature difference between upper and lower surfaces

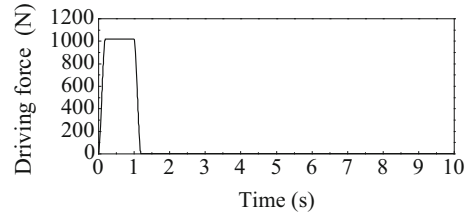


**Fig. 5** Time history of the driving force  $F_M$

According to the sunrise thermal environment described in Sect. 2.4, the temperature difference between upper and lower surfaces is shown in Fig. 4. In addition, the satellite is applied with a driving force to do translational motion in the Y direction. The time history of the force as shown in Fig. 5 is given by

$$F_M = \begin{cases} f_m \times t^2 / 0.2^2 \times (3 - 2t / 0.2) & 0 \leq t \leq 0.2 \\ f_m & 0.2 < t \leq 1 \\ f_m - f_m \times (t - 1)^2 / 0.2^2 \\ \quad \times (3 - 2 \times (t - 1) / 0.2) & 1 < t \leq 1.2 \\ 0 & t > 1.2 \end{cases} \quad (62)$$

where  $f_m = 1017.5 \text{N}$ .

## 7 Results and discussion

### 7.1 Parameter determination and effect of connection type

Thermally induced vibration of the whole system occurs along with the thermal dynamic forces great change (see Fig. 4). The satellite attitude shocks obviously due to the change of torsional spring torque and lock torque during the increase in sunrise thermal load. The torsional spring torque is proportional to the deployment angle according to Eq. (1). The thermal bending moment produced with the appearance of sunrise thermal load disturbs the solar array system and affects the deployment angle between the panel and

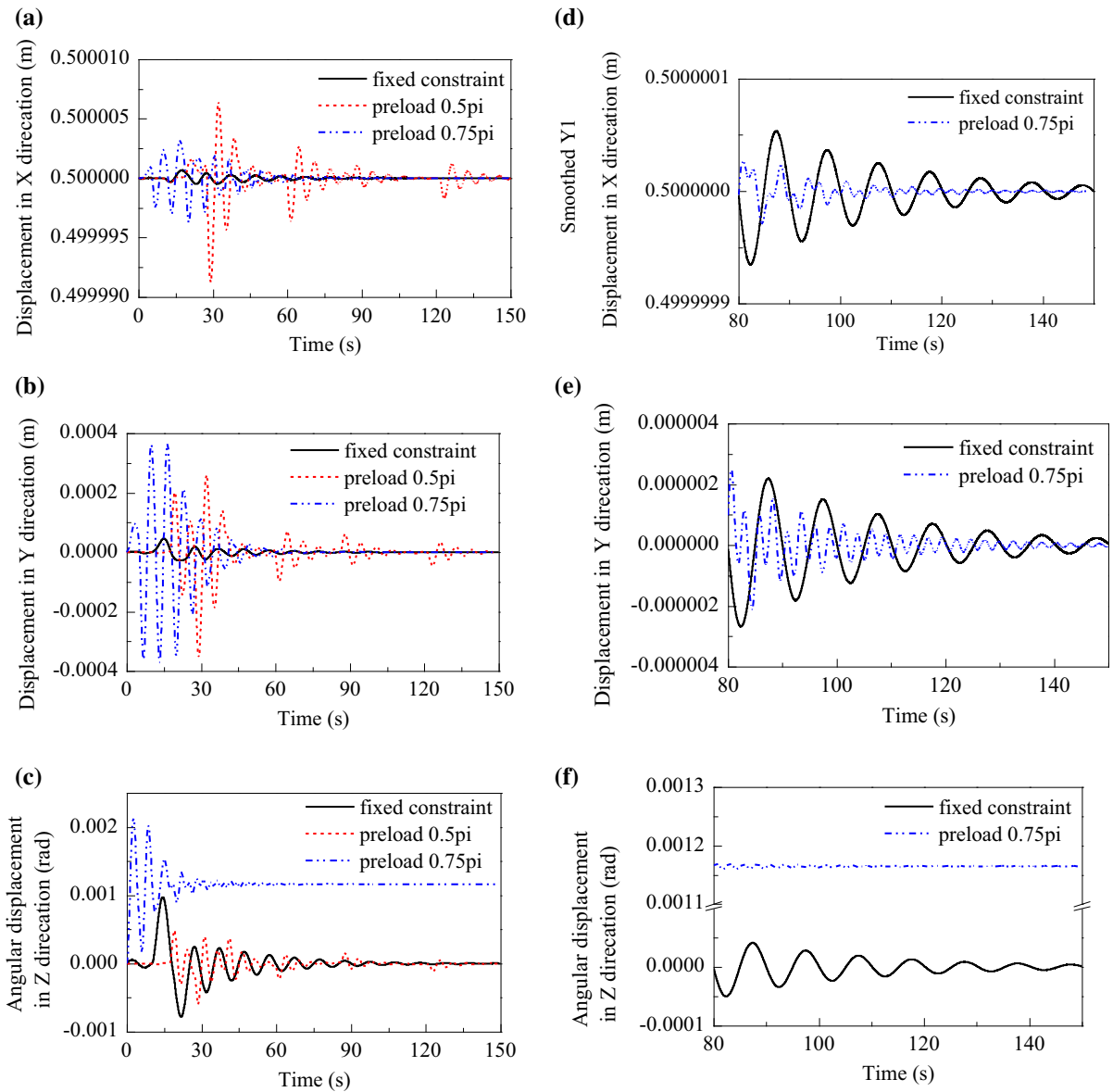


**Fig. 6** Effects of connection type and preload on spacecraft attitude

main body, which further makes the torsional spring torque and lock torque change dramatically.

To determine the parameter of the torsional spring mechanism, Figs. 6 and 7 give the comparison results of the effects on spacecraft attitude and solar panel, respectively. Obviously, the attitude yaw of the system connected by revolute joint with  $0.5\pi$  preload angle shows violent shock, and the solar panel appears high-amplitude rocking motions, due to the sequential instantaneous bilateral impact force from latch mech-

anism, as shown in Fig. 8, while the lock torque of the system with  $0.75\pi$  preload angle is unilateral and significantly decrease under the controller. It means that the system without preload margin of torsional spring cannot be controlled available. The pine of latch mechanism connected to panel make reciprocating motion between two sides of the groove in-wall of latch mechanism due to the bilateral collision, as the deployment angle shown in Fig. 9. By contrast, in the system whose torsional spring with  $0.75\pi$  preload angle, the pin can

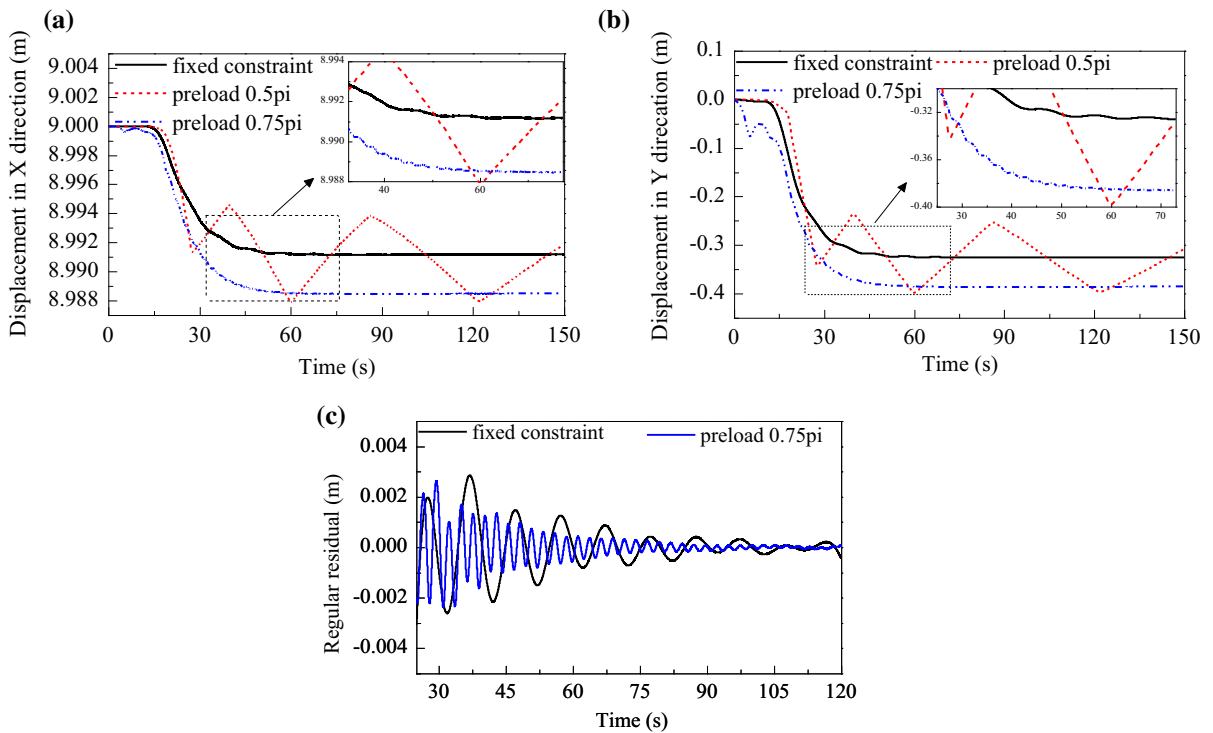


Fig. 7 Effects of connection type and preload on dynamics of solar panel

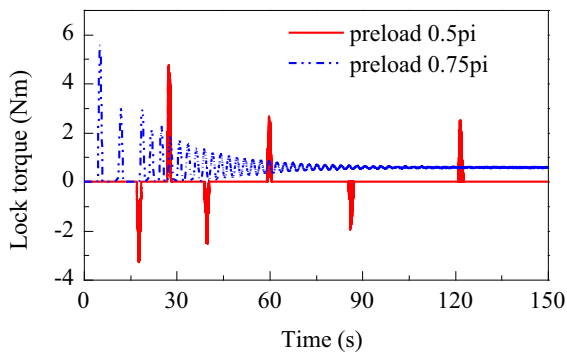


Fig. 8 Effect of different preloads on lock torque

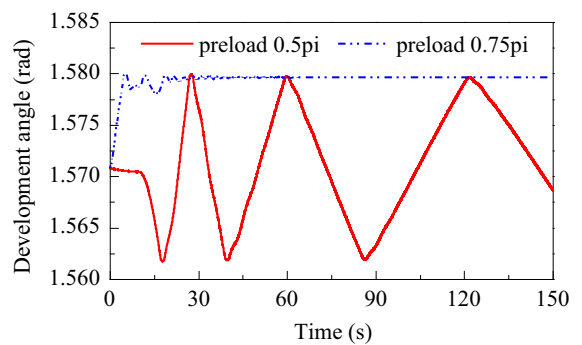


Fig. 9 Effect of different preloads on deployment angle

be repressed to one side in the latch mechanism and the solar panel would not make high-amplitude rocking motions to further disturb the spacecraft attitude. Obviously, the system with some preload margin shows greater stability performance on dynamics of spacecraft attitude and solar panel and can be effectively suppressed to avoid unnecessary shock under the controller. Thus, torsional spring with  $0.75\pi$  preload angle is applied to the models with revolute joint used in the following sections.

To compare the effects of the system with different connection types on spacecraft attitude, results of the system with fixed constraint and revolute joint are given in Fig. 6. The spacecraft attitude in X direction and Y direction of the system connected by revolute joint appears obviously larger-amplitude and higher-frequency oscillation than the system connected by fixed constraint during the thermal load great change stage. Because the system connected by revolute joint considers more comprehensive mechanism system and

introduces more disturbing forces, such as the lock torque from latch mechanism and torsional torque from spring mechanism. Besides, the amplitude and frequency of attitude angle yaw in Z direction of the system with revolute joint increase to some extent compared with the system connected by fixed constraint. Because the attitude angle here is mainly disturbed by additional torsion spring torque suppressed by the preload margin of the torsional spring. And affected by preload margin of the torsional spring, the attitude angle of the system under solar radiation cannot navigate to the desired location (0rad) under the attitude controller (see Fig. 6c). There is still a small rotation angle deviation of the satellite attitude (about 0.001162rad), that should be considered in the future controller design. Then the system enters the stable vibration period along with the thermal load into plateau after about 60s. The satellite attitude of the system with revolute joint maintains smaller-amplitude and higher-frequency jitter than the system with fixed constraint during the stable stage, as shown in Fig. 6d, e. Because the system with rev-

olute joint involves the damping property from additional mechanisms to attenuate vibration amplitude and more disturbance sources to influence vibration frequency.

Similarly, solar panel of the system with revolute joint shocks obviously during the thermal great change stage, compared to the system with fixed constraint, as shown in Fig. 7. And as the temperature difference between upper and lower surfaces reaches the plateau, the amplitude of thermally induced vibration of solar panel with revolute joint decreases, but the frequency increases compared with the system with fixed constraint.

### 7.2 Effects on satellite attitude

Figures 11 and 12 give the dynamic response of satellite attitude of these six comparison models to study the effects of sunrise thermal load, attitude adjustment load, and joint clearance on the spacecraft attitude.

Comparing Figs. 10, 11 and 12a, b, effects of the appearance of clearance joint on satellite attitude can

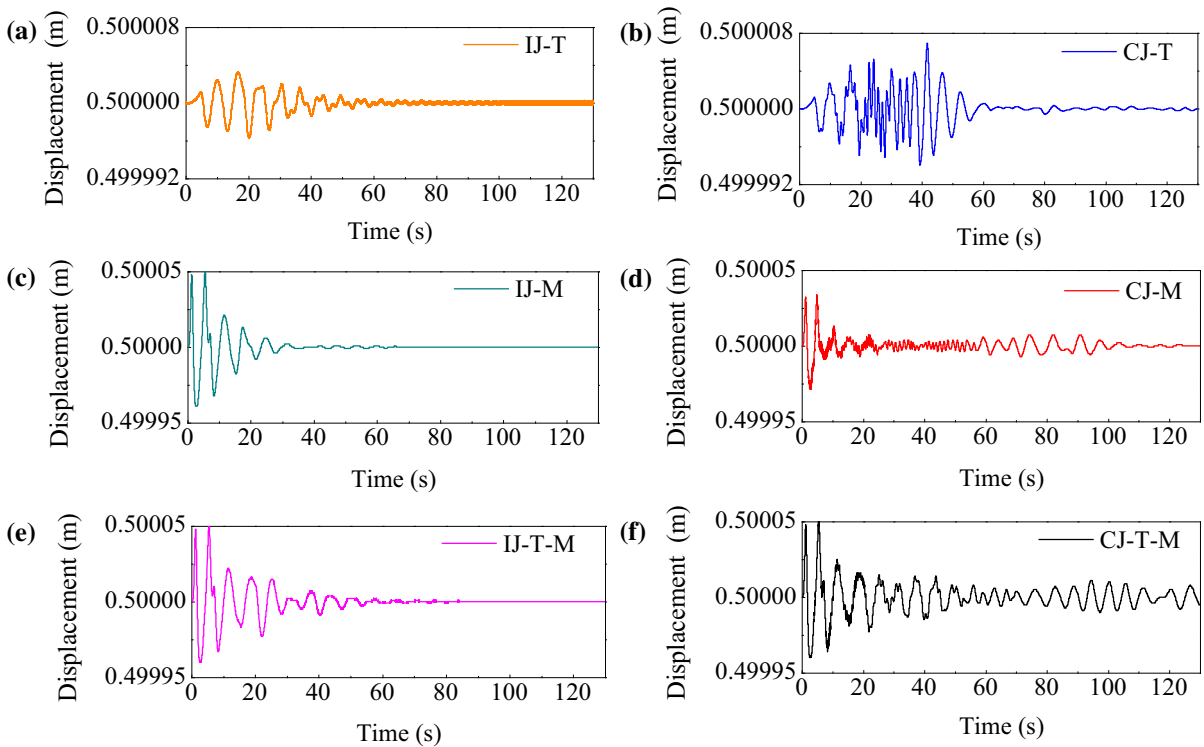


**Fig. 10** Displacement in X direction of spacecraft main body

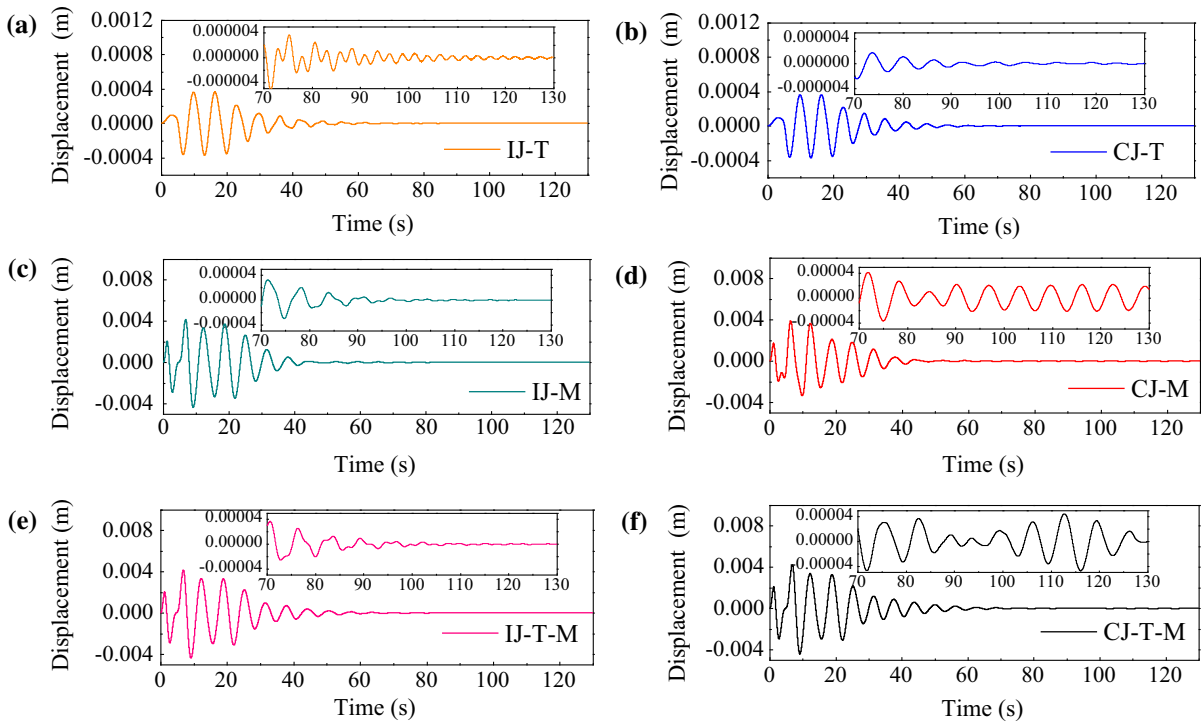


**Fig. 11** Relative displacement in Y direction of spacecraft main body

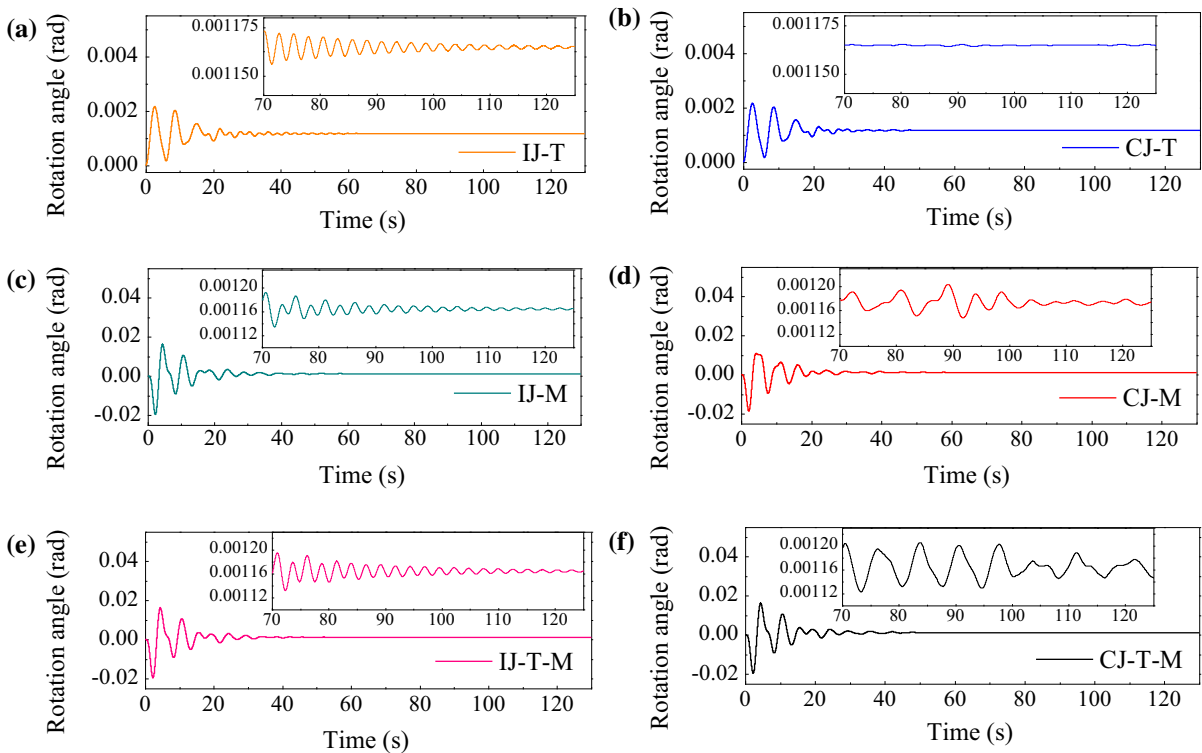


**Fig. 12** Rotation angle in Z direction of spacecraft main body



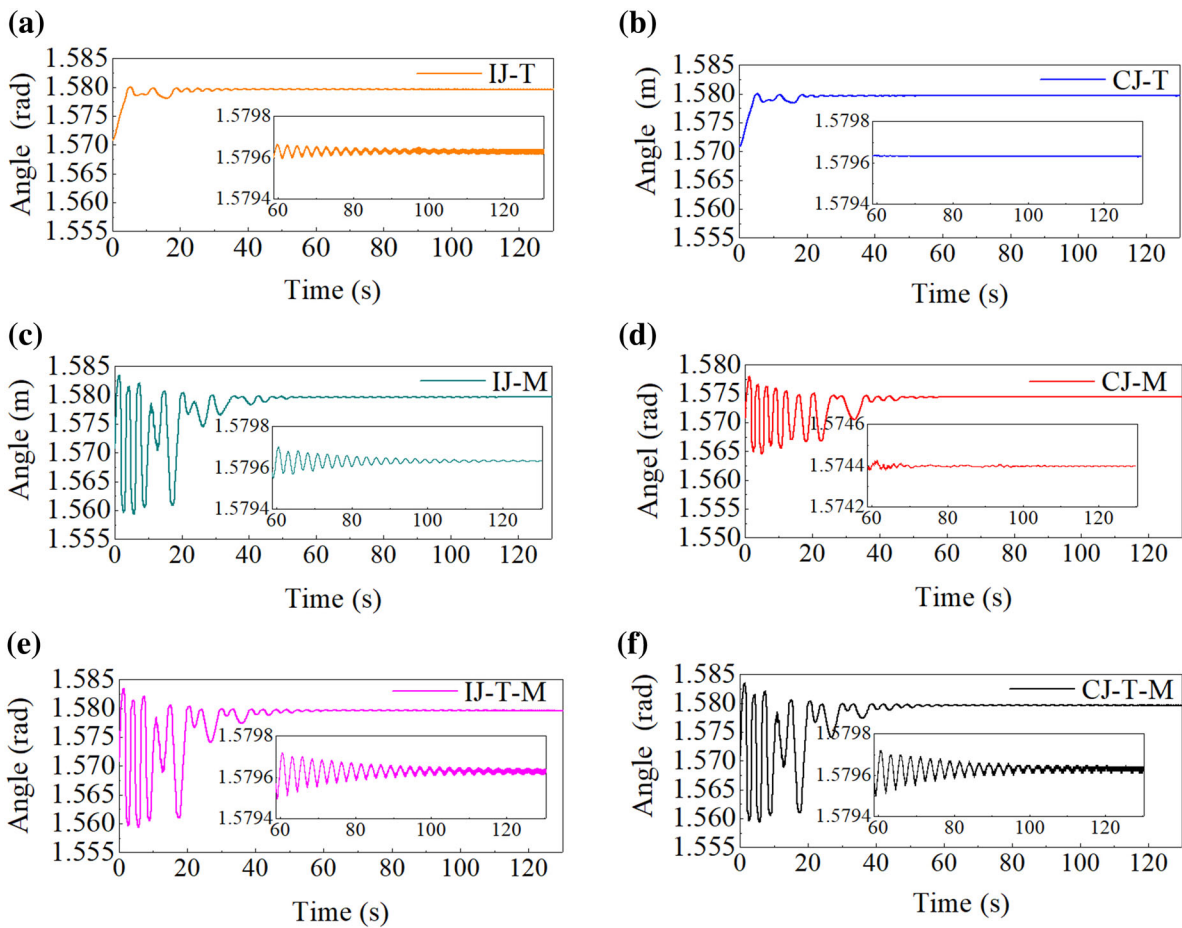


**Fig. 13** Deployment angle between spacecraft main body and solar panel

be obtained under the thermal environment. Affected by the contact and impact force generated at joint clearance, the yaw amplitude of satellite attitude increases to a certain extent along with the rise of sunrise thermal load, especially in X direction as shown in Fig. 10b. However, as the heat load enters the plateau after 60 s, the yaw shock of satellite attitude of the system with clearance joint reduces significantly than that of the system with ideal joint. The clearance joint acts as a suspension damping to steady the system at this steady phase of heat load, when the thermal stress causes a small range of vibration of the whole system. The suspension damping property blocks the transmission of thermally induced vibration of the solar array to spacecraft main body. Thus, the shock frequency becomes considerably lower and the shock amplitude decreases obviously as shown in Fig. 11b. Here the system shocks

mainly due to the disturbance from contact force at clearance joints. Similarly, after 60 s, the deployment angle and lock torque of the system with clearance joint stay within a small numerical range and evidently avoid the vibration generated from thermal effect due to the suspension damping property of the joint clearance (see Figs. 13b, 14b), compared with these of the system with ideal joint (see Figs. 13a, 14a). It is worth pointing out that due to the decrease in vibration amplitude of the torsional spring torque acted on spacecraft main body, the rotation angle attitude error of the system with clearance joint has dramatic improvement and can be controlled within an almost perfect range as shown in Fig. 12b.

As shown in Figs. 10, 11 and 12c) elastic vibration coupled with overall motion, panel flexibility brings the obvious oscillation into the solar array system to

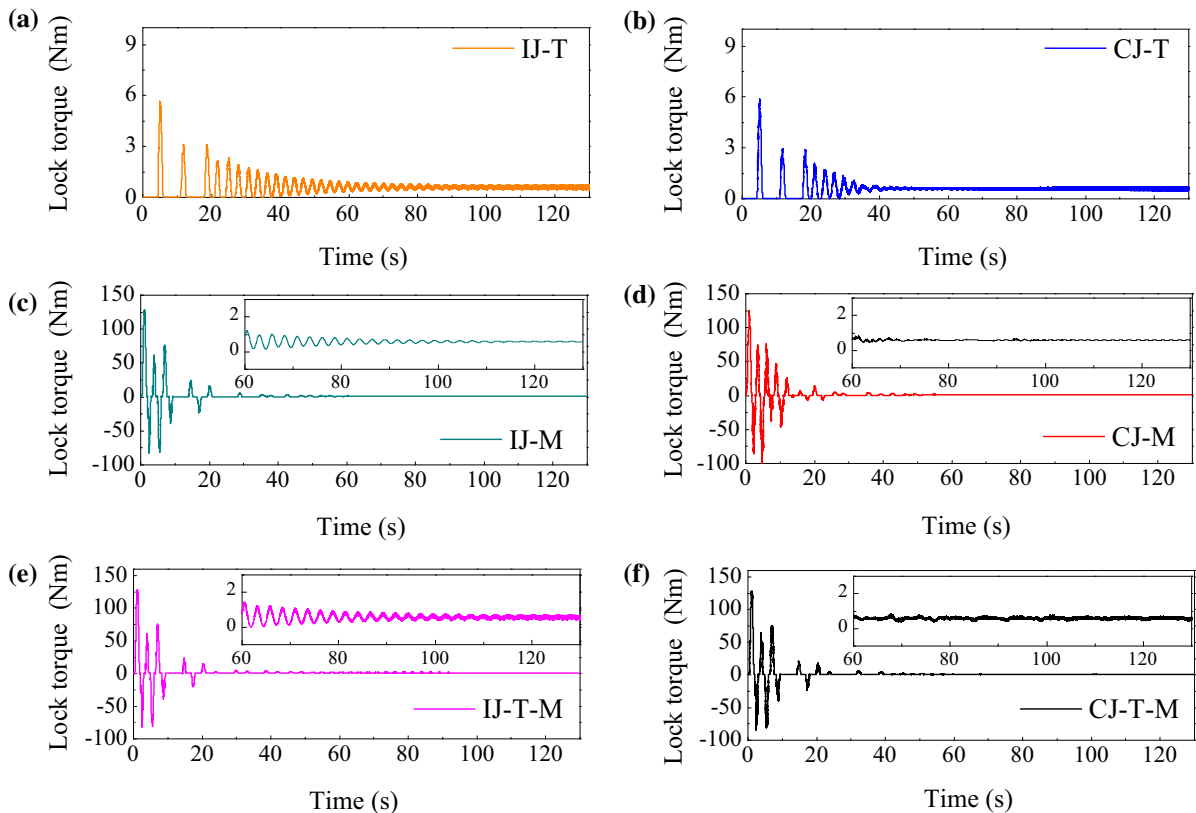


**Fig. 14** Lock torque of these six comparison models

disturb the satellite attitude. The oscillation amplitude brought by this translational motion is about an order of magnitude larger than that of the system just considering thermal environment effect. The solar array system gradually becomes stable without the sustained action of driving force  $F_M$  under the attitude controller as well.

Similarly, as can be seen in Figs. 10d and 11d, the contact force generated at clearance joint make some instantaneous impacts to disturb the attitude of the satellite, especially in X direction. In addition, the existence of joint clearance significantly reduces the change of deployment angle between the spacecraft main body and solar panel by comparing Fig. 13c, d. Thus, the yaw of rotation angle in Z direction of the system with clearance joint (see Fig. 12d) is apparently lower than that of the system with ideal joint (see Fig. 12c) during the sharp adjustment stage about 0–40s, due to the decreased dithering amplitude of torsional spring torque acted on spacecraft main body, which is proportional to deployment angle. However,

when the system enters steady adjustment stage, the contact force takes place of lock torque and torsional spring torque to become the dominant disturbance force for the system with clearance joint. Because of that, the satellite attitude of the system with clearance joint has more drastic change than that of the system with ideal joint during the steady operation stage as shown in partial enlarged drawings of Figs. 10, 11 and 12d, although the lock force and torsional spring torque of the clearance system during this stage are also smaller than these of the ideal system as shown in Figs. 13 and 14d.

Considering both the thermal load and overall adjustment motion, Figs. 10, 11 and 12a, c, e show that the degree of yaw jitter of the system with ideal joint might be seen as a superposition to a certain extent, which is the sum of thermally induced vibration error plus elastic vibration error caused by motion. However, for the clearance joint system, the thermal load coupled with overall adjustment motion bring dramatic and violent shaking to the satellite attitude and the shaking

will last for a long time, as shown in Figs. 10, 11, and 12d. The combined effect of thermal load and overall motion on dynamic response of satellite attitude is absolutely no longer the simple superposition action by comparing Figs. 10, 11 and 12b, d, f clearly. Comparing Figs. 10e, 11e and 12e and 10f, 11f and 12f, the coupling of thermal load and overall motion excites the instability of the solar array system. At the whole simulation process, the enhanced contact force becomes dominant disturbance for the satellite attitude control. The yaw amplitude of attitude of the system with clearance joint is obviously larger than that of the system with ideal joint, although the torsional spring torque and lock torque of the clearance model are not increase, as shown in Figs. 13 and 14d. The suspension damper property of the joint clearance decreases the high-frequency jitter of the satellite attitude affected by flexible panel vibration, but meanwhile, the contact force generated at clearance joint increases the high-amplitude low-frequency jitter of the satellite attitude.

And the system with clearance joint considering thermal load and adjustment motion cannot get stability for quit a long time.

### 7.3 Effects on solar panel

Figures 15 and 16 give the dynamic response of point P (see Fig. 1) of these six comparison models to study the effects of sunrise thermal load, attitude adjustment load, and joint clearance on solar panel.

Figures 15a and 16a give the effect of solar radiation environment on the solar panel. The thermal bending moment make the panel has a large bending deflection, which grows with the increase of the temperature difference between upper and lower surfaces, until the temperature difference reaches stable. Meanwhile, thermally induced vibration phenomenon happens and the vibration will gradually subside over time.

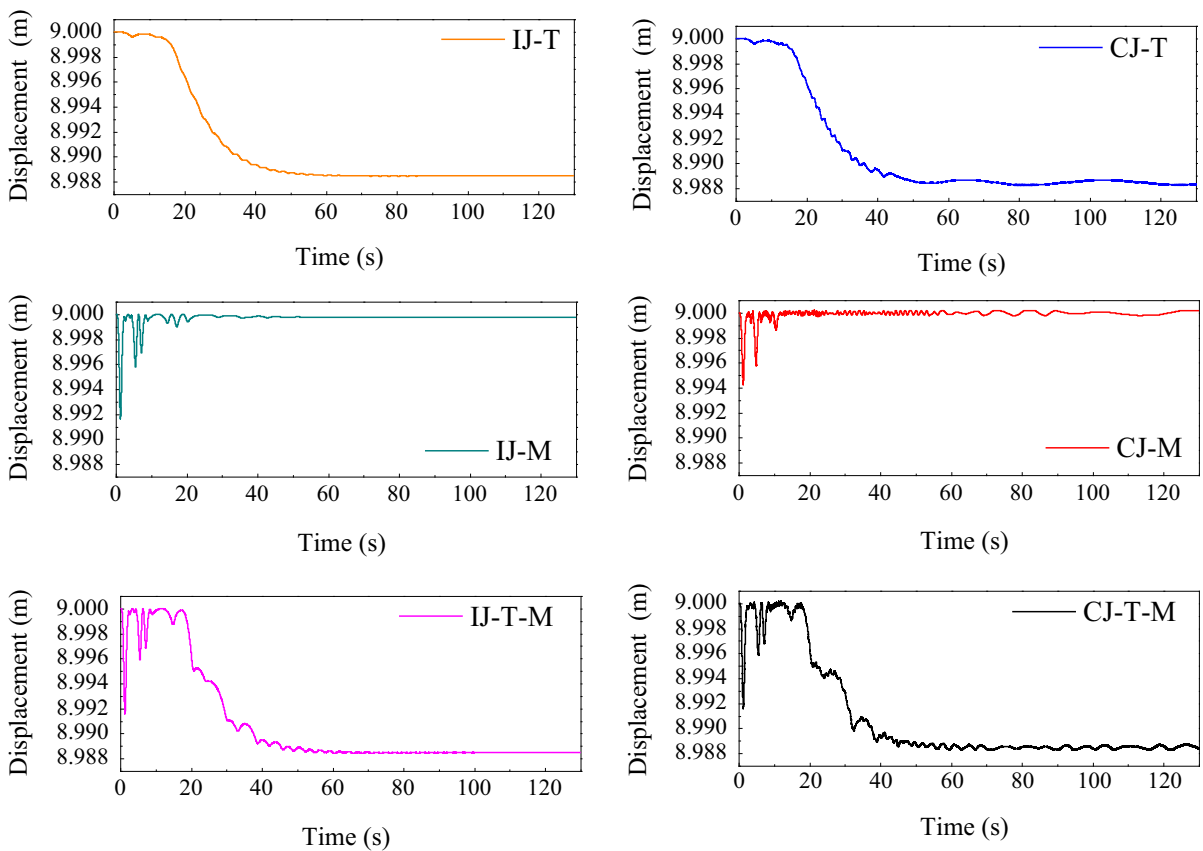
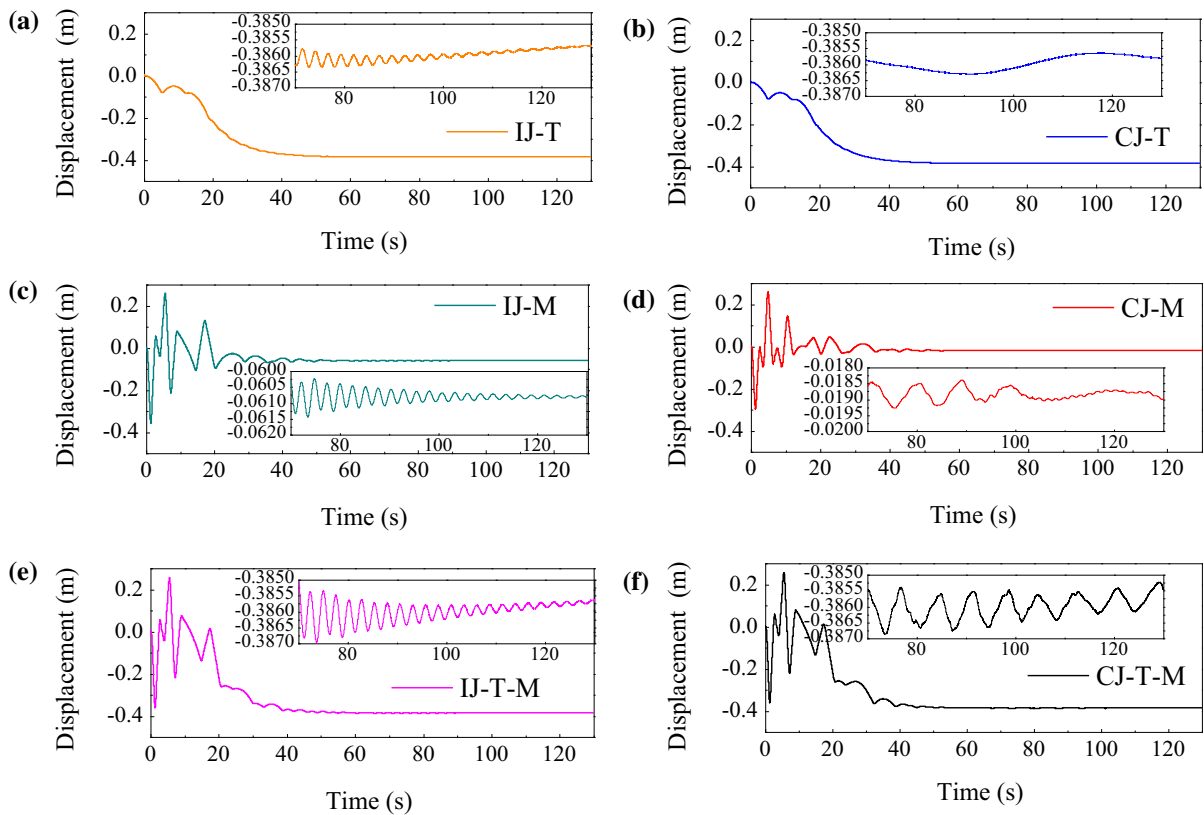


Fig. 15 Displacement in X direction of point P



**Fig. 16** Relative displacement in Y direction of point P

Compared with Figs. 15b and 16b, the system with clearance joint avoids the high-frequency phenomenon and just retains a large bending deflection of solar panel. Because the suspension damper property of joint clearance blocks the thermally induced vibration of the panel due to the suspension damper property. But the existence of joint clearance makes the solar panel have an overall waggle as a result of that the hinge pin can free flight within the inner wall of sleeve. Figure 17a shows the relative movement locus between the center of hinge pin and the center of the sleeve at the clearance joint of the system considering sunrise thermal load. Hinge pin impact sleeve violently during the great change stage of the thermal dynamic forces and then hinge pin enters the free flight mode along with the thermal load becomes stable after about 60s.

Similarly, overall translation motion excites the elastic vibration of the large flexible solar panel, as shown in Figs. 15c and 16c. The solar panel shocks obviously due to the sudden action of the driving force and then gradually becomes stable when the system no

more acted by the driving force. The vibration amplitude brought by this translational motion is about twice than that of the system just considering thermal environment effect. The steady value of the panel vibration in Y direction is slightly less than 0. Because the preload of torsional spring makes the deployment angle larger than  $0.5\pi$ , as shown in Fig. 13c.

Figures 15d and 16d show the deflection of the solar panel of the system with clearance joint considering translational motion. Due to the decrease in the fluctuation degree of deployment angle as shown in Fig. 13d, the maximum amplitude of the panel oscillation of the system with clearance joint reduces during the great change of driving force. In addition, at the system stable stage, as shown in partial enlarged drawing of Fig. 16d, the solar panel make high-amplitude and low-frequency oscillation due to the collision motion at clearance joint coupled with low-amplitude and high-frequency vibration due to the elastic vibration of flexible panel reduced by suspension damping. Then the oscillation of the solar panel decays as the collision

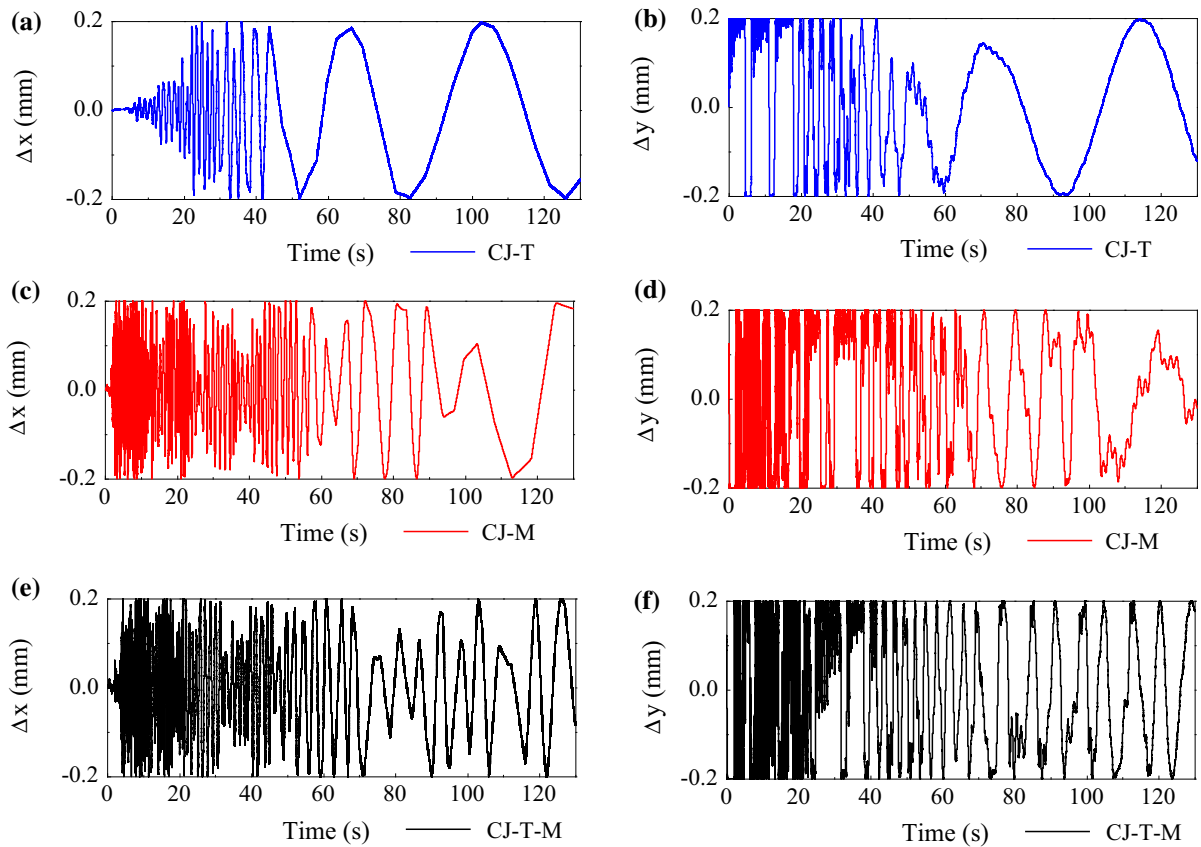


**Fig. 17** Relative movement locus in X direction and Y direction with time

motion weakens over time. Figure 17c, d shows the collision motion locus at the clearance joint of the system considering overall motion. The existence of joint clearance reduces the deviation of deployment angle generated from the preload of torsional spring to make the panel closer to the horizontal.

Comparing Figs. 15 and 16a, c, e, for the ideal joint system, the vibration degree of the solar panel considering both sunrise thermal load and oval motion might be also seen as the superposition of the vibrations excited by each situation. However, for the clearance joint system, the vibration degree of the solar panel increases obviously, as shown in Figs. 15f and 16f. Vibration amplitude and vibration duration of the solar panel considering both thermal load and adjustment force occur nonlinear changes and far beyond these of the system just considering one load condition (see Figs. 15, 16b, d). Obviously, coupling effect of the thermal load and overall motion on the dynamics of clearance joint system is not simply superposition of each single effect,

which causes the dramatic shake of the solar panel and is difficult to be controlled into stability, although the suspension damper property of the clearance joint can effectively attenuate elastic vibration of the flexible panel compared to the ideal joint system.

#### 7.4 Effect on joint wear

Some results of these three comparison models (Model CJ-T, Model CJ-M, and Model CJ-T-M) are shown to study the effect of sunrise solar radiation, overall motion and their coupling on the wear degree of the system with clearance joint.

To better understand the action of clearance joint under different operation conditions, Fig. 18 shows the hinge pin center locus of clearance joints of these three comparison models after 60s. Only considering the sunrise thermal load condition, the hinge pin center locus is concise and little collision occurs between

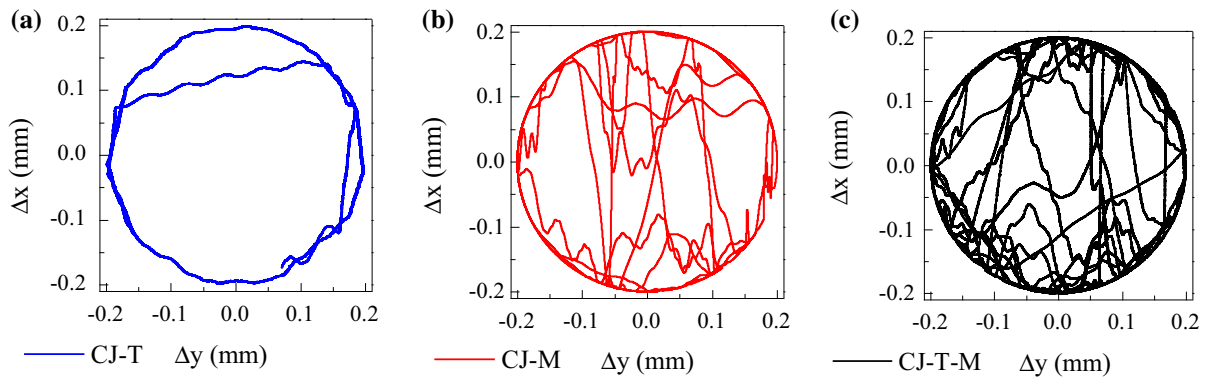


**Fig. 18** Hinge pin center locus of clearance joint

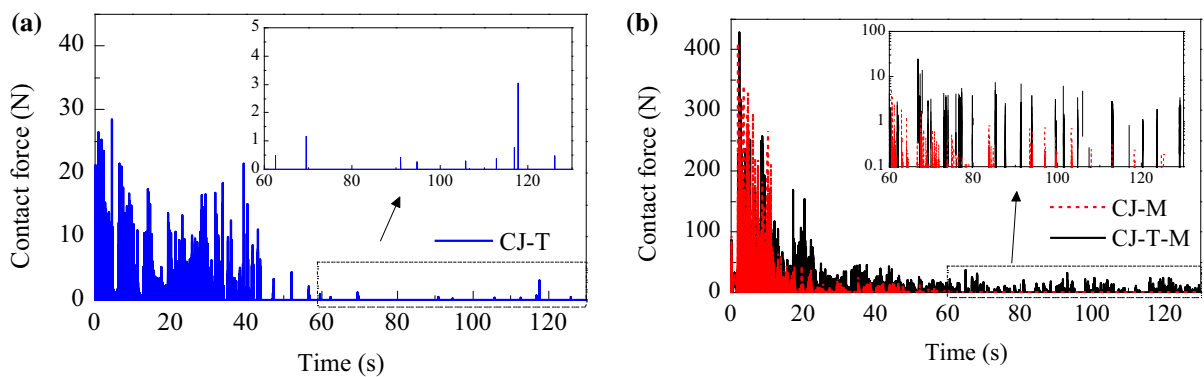


**Fig. 19** Contact force at clearance joint

the hinge pin and the inner wall of sleeve, as shown in Fig. 18a. The corresponding contact force is shown in Fig. 19a. At the great change stage of temperature difference between upper and lower surface, the contact force is large and intense. With the stabilization of the temperature difference, the contact force becomes few and scattered after 60s. When just considering the overall motion condition, the adjustment driving force arouses the significant vibration of the system and the collision at clearance joint is obviously intense (see Fig. 18b). The maximum contact force under the sudden overall motion almost increases by one order of magnitude than that under the solar radiation, as red line shown in Fig. 19b.

However, considering both thermal load and overall adjustment motion, the coupling effect stimulates the system shake dramatically. The collision frequency is significantly denser and the impact trace becomes more disordered than the simple superposition of each single condition, as shown in Fig. 18c. Obviously, coupled

with the sunrise thermal load effect, the contact force is larger than that just considering adjustment motion, as shown in Fig. 19b. And, more remarkable, although the temperature difference has reached a plateau, the impact is still significant and lasting. Partial enlarged drawing of Fig. 19b gives the comparison detail that the contact force of the system under the coupling effects is much denser and an order of magnitude greater than that of the system without considering thermal load.

To compare the wear degree at clearance joint of the system under different operation conditions, Fig. 20 shows the wear depth of clearance joint with and without the coupled thermal load effect. Obviously, the wear depth of Model CJ-T-M increases about two orders of magnitude than that of the model neglecting the effect of solar radiation. For the solar array system with clearance joint, wear prediction error at the order of magnitude degree might appear when the simulation ignores the thermal load. Although effect of thermal load on



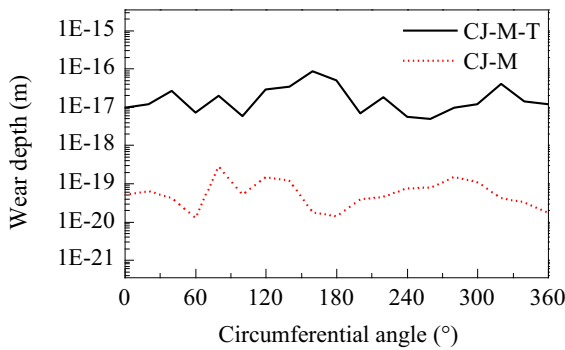


**Fig. 20** Effect of thermal load on wear depth

wear at clearance joint of a stationary system is little, which is unrealistic for the spacecraft carrying out mission, the effect of the thermal load combined with the adjustment motion is huge and significant on the clearance joint of the solar array system.

## 8 Conclusions

This paper establishes more comprehensive rigid-flexible-thermal solar array model considering torsional spring, latch mechanism, and attitude controller, involves ideal revolute joint to reveal the effects of the connection type between spacecraft and solar panel compared with the fixed constraint generally used in previous studies, and introduces clearance revolute joint to study the effects of solar radiation, overall adjustment motion and their coupling on the dynamic performance of the system in detail, including satellite attitude, solar panel response, and wear prediction. The rigid-flexible-thermal dynamical equation is derived based on NCF-ANCF formulation and solved by generalized- $\alpha$  method. The nonlinear Lankarani–Nikravesh model, amendatory Coulomb friction model, and Archard's wear model are applied to establish the clearance joint and to evaluate the wear degree.

A certain preload margin is necessary for the torsional spring mechanism design, that make the system avoid additional oscillations stimulated from latch torque and make the shake of the system can be attenuated effectively under the attitude controller. During the sunrise load change stage, the yaw amplitude and frequency of the system connected by revolute joint significantly increase compared with the system with

fixed constraint, especially in X and Y directions, due to the more disturbance force from torsional spring and latch mechanism. Although the more damping terms are also introduced to the system to reduce the shake amplitude during the stable stage, the effect of connection using revolute joint on the maximum yaw of spacecraft attitude under thermal environment is cannot be ignored. Besides, the preload margin may influence the attitude angle accuracy of the spacecraft under the thermal environment, that should gain attention in attitude controller design.

Furthermore, as for the effects on the satellite attitude, when just considering solar thermal environment, the contact force generated at clearance joint intensifies attitude yaw during the great change stage of thermal load, while the suspension damper property of clearance joint blocks the influence from high-frequency thermally induced vibration of large solar panel on the satellite attitude after the thermal load into stable stage. And considering the overall translational motion only, the relevant torques, such as torsional spring torque, whose change amount is weakened due to joint clearance, reduce the maximum yaw value of the system at the strong shake stage. Conversely, as the system enters the stable stage, contact and impact force at clearance joint play the dominant role to make the clearance system more shocker than the ideal joint system. Most of all, when we consider both thermal environment and overall motion conditions, for the ideal joint system, the attitude yaw degree can be seen as a superposition of each single-condition-induced shake. However, the attitude yaw of the system with clearance joint increases dramatically, and the degree and duration of the shake far beyond the superposition of each single condition.

Similarly, considering two conditions separately, solar panel of the system with clearance joint can avoid high-frequency jitter as a result of that the joint clearance as a suspension damper can absorb the motion-induced vibration and thermal-induced vibration of the flexible panel, and replace them with smoother and low-frequency swing due to the free motion of hinge pin at clearance joint. However, although the joint clearance weakens the high-frequency elastic vibration of the panel, the coupling effect of the thermal load and overall motion on the system with clearance joint excites solar panel to make large amplitude shake and the shake is hard to be suppressed for a long time.

Coupling effect of solar radiation environment and overall adjustment motion causes considerable oscillation to the imperfect system. After the spacecraft making adjustment motion, the contact force at clearance joint of the system considering solar radiation environment is much more intensive and becomes ten times larger than that of the system without considering thermal environment. The wear degree of clearance joint combined with the effect of thermal environment increases two orders of magnitude after spacecraft adjustment motion. Although the wear caused only by steady thermal load is little, the coupling effect of thermal environment on the wear prediction of the solar array system is non-negligible.

These results reveal that the existence of joint clearance and effect of thermal environment should be considered simultaneously into on-orbit solar array system. To ensure the normal and safe operation of spacecraft, it is necessary to pay attention to some coupling effects, that may provide valuable references for controller design and reliability analysis. The solar array system with more integrated configurations and multiple clearance joints may be considered in the further work.

**Acknowledgements** This work is supported by the National Natural Science Foundation of China (U1637207). The author Yuan Yuan Li acknowledges the support from China Scholarship Council (CSC) and the kind help from Prof. Mathias Legrand.

#### Compliance with ethical standards

**Conflict of interest** The authors declare that they have no conflict of interest.

#### References

1. Thornton, E.A., Kim, Y.A.: Thermally induced bending vibrations of a flexible rolled-up solar array. *J. Spacecr. Rockets* **30**(4), 438–448 (1993)
2. Thornton, E.A., Foster, R.S.: Dynamic response of rapidly heated space structures. *Computational Nonlinear Mechanics in Aerospace. Engineering* **146**, 451–477 (1992)
3. Thornton, E.A., Chini, G.P., Gulick, D.W.: Thermal induced vibrations of a self-shadowed split-blanket solar array. *J. Spacecr. Rockets* **32**, 302–311 (1995)
4. Foster, C.L., Tinker, M.L., Nurre, G.S., Till, W.A.: The solar array-induced disturbance of the Hubble Space Telescope pointing system. *NASA STI/Recon Tech. Rep. N* **95**, 1–36 (1995)
5. Li, J.L., Yan, S.Z., Cai, R.Y.: Thermal analysis of composite solar array subjected to space heat flux. *Aerosp. Sci. Technol.* **27**, 84–94 (2013)
6. Li, J.L., Yan, S.Z.: Thermally induced vibration of composite solar array with honeycomb panels in low earth orbit. *Appl. Therm. Eng.* **71**(1), 419–432 (2014)
7. Shen, Z.X., Tian, Q., Liu, X.N., Hu, G.K.: Thermally induced vibrations of flexible beams using absolute nodal coordinate formulation. *Aerosp. Sci. Technol.* **29**, 386–393 (2013)
8. Liu, J., Pan, K.: Rigid-flexible-thermal coupling dynamic formulation for satellite and plate multibody system. *Aerosp. Sci. Technol.* **52**, 102–114 (2016)
9. Liu, L., Cao, D., Huang, H., et al.: Thermal-structural analysis for an attitude maneuvering flexible spacecraft under solar radiation. *Int. J. Mech. Sci.* **126**, 161–170 (2017)
10. Azadi, E., Fazelzadeh, S.A., Azadi, M.: Thermally induced vibrations of smart solar panel in a low-orbit satellite. *Adv. Space Res.* **59**(6), 1502–1513 (2017)
11. Bai, J.B., Sheno, R.A., Xiong, J.J.: Thermal analysis of thin-walled deployable composite boom in simulated space environment. *Compos. Struct.* **173**, 210–218 (2017)
12. Yaqubi, S., Dardel, M., Daniali, H.M., et al.: Modeling and control of crank-slider mechanism with multiple clearance joints. *Multibody Syst. Dyn.* **36**(2), 143–167 (2016)
13. Flores, P., Ambrósio, J., Claro, J.C.P., et al.: Lubricated revolute joints in rigid multibody systems. *Nonlinear Dyn.* **56**(3), 277–295 (2009)
14. Flores, P., Koshy, C.S., Lankarani, H.M., Ambrósio, J., Claro, J.C.P.: Numerical and experimental investigation on multibody systems with revolute clearance joints. *Nonlinear Dyn.* **65**(4), 383–398 (2011)
15. Erkaya, S., Doğan, S., Ulus, Ş.: Effects of joint clearance on the dynamics of a partly compliant mechanism: numerical and experimental studies. *Mech. Mach. Theory* **88**, 125–140 (2015)
16. Koshy, C.S., Flores, P., Lankarani, H.M.: Study of the effect of contact force model on the dynamic response of mechanical systems with dry clearance joints: computational and experimental approaches. *Nonlinear Dyn.* **73**(1–2), 325–338 (2013)
17. Flores, P., Lankarani, H.M.: Dynamic response of multibody systems with multiple clearance joints. *J. Comput. Nonlinear Dyn.* **7**(3), 031003 (2012)
18. Erkaya, S., Doğan, S., Şefkatlıoğlu, E.: Analysis of the joint clearance effects on a compliant spatial mechanism. *Mech. Mach. Theory* **104**, 255–273 (2016)
19. Wang, Z., Tian, Q., Hu, H., et al.: Nonlinear dynamics and chaotic control of a flexible multibody system with uncertain joint clearance. *Nonlinear Dyn.* **86**(3), 1571–1597 (2016)
20. Zhang, L.X., Bai, Z.F., Zhao, Y., et al.: Dynamic response of solar panel deployment on spacecraft system considering joint clearance. *Acta Astronaut.* **81**(1), 174–185 (2012)
21. Li, J., Yan, S., Guo, F., et al.: Effects of damping, friction, gravity, and flexibility on the dynamic performance of a deployable mechanism with clearance. *Proc. Inst. Mech. Eng. Part C J. Mech. Eng. Sci.* **227**(8), 1791–1803 (2013)
22. Li, Y., Wang, Z., Wang, C., et al.: Dynamic responses of space solar arrays considering joint clearance and structural flexibility. *Adv. Mech. Eng.* **8**(7), 1–11 (2016)

23. Li, H.Q., Liu, X.F., Duan, L.C., et al.: Deployment and control of spacecraft solar array considering joint stick-slip friction. *Aerosp. Sci. Technol.* **42**, 342–352 (2015)
24. Li, H.Q., Duan, L.C., Liu, X.F., et al.: Deployment and control of flexible solar array system considering joint friction. *Multibody Syst. Dyn.* **39**(3), 249–265 (2017)
25. Li, Y., Wang, Z., Wang, C., et al.: Planar rigid-flexible coupling spacecraft modeling and control considering solar array deployment and joint clearance. *Acta Astronaut.* **142**, 138–151 (2018)
26. Li, Y., Wang, Z., Wang, C., et al.: Effects of torque spring, CCL and latch mechanism on dynamic response of planar solar arrays with multiple clearance joints. *Acta Astronaut.* **132**, 243–255 (2017)
27. Johnston, J.D., Thornton, E.A.: Thermally induced dynamics of satellite solar panels. *J. Spacecr. Rockets* **37**(5), 604–613 (2000)
28. Shabana, A.A.: Definition of the slopes and the finite element absolute nodal coordinate formulation. *Multibody Syst. Dyn.* **1**, 339–348 (1997)
29. Li, T., Wang, Y.: Deployment dynamic analysis of deployable antennas considering thermal effect. *Aerosp. Sci. Technol.* **13**, 210–215 (2009)
30. Liu, C., Tian, Q., Hu, H.: Dynamics of a large scale rigid-flexible multibody system with composite laminated plates. *Multibody Syst. Dyn.* **26**, 283–305 (2011)
31. Johnston, J.D., Thornton, E.A.: Thermally induced attitude dynamics of a spacecraft with a flexible appendage. *J. Guid. Control Dyn.* **21**(4), 581–587 (1998)
32. Lankarani, H.M., Nikravesh, P.E.: A contact force model with hysteresis damping for impact analysis of multibody systems. *J. Mech. Des.* **112**(3), 369–376 (1990)
33. Archard, J.F.: Contact and rubbing of flat surfaces. *J. Appl. Phys.* **24**(8), 981–988 (1953)
34. Lai, X., He, H., Lai, Q., et al.: Computational prediction and experimental validation of revolute joint clearance wear in the low-velocity planar mechanism. *Mech. Syst. Signal Process.* **85**, 963–976 (2017)
35. Zhu, A., He, S., Zhao, J., et al.: A nonlinear contact pressure distribution model for wear calculation of planar revolute joint with clearance. *Nonlinear Dyn.* **88**(1), 315–328 (2017)

**Publisher's Note** Springer Nature remains neutral with regard to jurisdictional claims in published maps and institutional affiliations.